学位論文

Doctoral Dissertation

Study on Calculation Method of Computer-Generated Hologram for Volume Data

ボリュームデータの計算機合成ホログラム計算法に関する研究

Zixiang Lu

盧　子祥

Graduate School of Information Science and Technology
Division of Media and Network Technologies
Hokkaido University

北海道大学大学院情報科学研究科
メディアネットワーク専攻

March 2019

Thesis advisor: Professor Yuji Sakamoto Zixiang Lu

Study on Calculation Method of Computer-Generated Hologram for Volume Data

Abstract

Volume data are widely used in many areas, especially biomedical science and geology. Visualizing volume data is very important to enable intuitive understanding of three-dimensional structures, making them easier to analyze. However, current visualization technologies of volume data cannot satisfy the requirements of humans. In this thesis, I propose three CGH calculation methods for volume data : polygon-based, MIP-based, and volume rendering based methods. In the polygon-based CGH calculation method, first I do the surface extraction. The CGHs of volume data were generated using a ray tracing method. In the MIP-based CGH calction method, I use a modified ray tracing method to generate holograms of MIP models. In volume rendering based CGH calculation method, I attempt to apply the diffuse reflection model to render the volume data. I calculate the CGHs for volume data using a point light based CGH method. I can display the reconstructed images and animations using an electro-holography device. These three methods can display the depth and motion parallax well. The polygon-based CGH calculation method can obtain clear reconstructed images, and I can combine the models with our own ideas by using the 3DCG editing softwares. The color and material of polygonal models can be designed independently. Compared with the polygon-based CGH calculation method, the MIP-based CGH calculation method can only generate a single-color hologram. Using the same series of volume data, the polygon-based CGH calculation method can generate a variety of holograms, can express the 3D sense of objects better than the MIP-based method. In addition, the materials of objects can be correctly expressed by the polygon-based method. The volume rendering based method can display the transparent objects and multi-layer objects well. Compared with polygon-based and MIP-based CGH calculation methods, the detail of holograms calculated by the volume rendering based CGH calculation method is better. For the computing speed, the MIP-based method is much faster than the polygon-based and volume rendering based CGH calculation methods. It is possible to generate the CGHs in real-time. The calculation time of volume rendering based method is very long. To increase the speed of calculation, I

propose an elemental holograms based CGH calculation method. And I reconstruct the holographic images on an eyepiece-type electro-holographic display device.

Contents

Listing of figures

List of Tables

1

Introduction

Currently, volume data are widely used in many areas, such as biomedical science [1], and geology. Volume data represent three-dimensional (3D) objects. And volume data are composed of a series of voxels. A voxel represents a value on a regular grid in 3D space. Generally, volume data can be generated by many measuring instruments, including magnet resonance imaging (MRI), computed tomography (CT), and meteo-

rological instrumentation.

In order to make volume data easy to understand, many excellent visualization technologies have been proposed in the field of computer graphics (CG), such as surface extraction algorithm [2], maximum intensity projection (MIP) [3], and volume rendering [4] [5]. According to different purposes of volume data, I can select different visualization method to use. The visualized images are very clear and easy to understand, but they are projections of CG models in a 2D plane, rather than a true 3D image.

1.1 Three dimensional display technologies

Since the 1980s, CG technology began to be used for movies and games. Currently, it is not limited to movies, and it is unreal in all television commercial images, illustration, cartoons, etc. The image created with this CG technology is made very realistically and there are many things that make it appear as if it is a real picture.

In addition, the high definition displays were developed, which can give a sense of reality by presenting detailed images with a large screen spreading before the eyes. However, there is no depth scene with these displays. In order to realize the super-realistic system, there are various technical problems and cooperation of many different fields is indispensable. Currently, the expectation entrusted to the super-realistic system is very large. In super-realistic system, 3D imaging technology is a very important role. It is required that not only display technology but also creation of contents and elucidation of the influence on human body and formulation of guidelines for using 3D video based on this will be urgently required.

1.1.1 Three dimensional perception

In CG area, the basic drawing data are substantially based on a three-dimensional x, y, and z-coordinates, but the information is converted to 2D for display on the 2D screen and other devices. Compared with 3D, this image is referred to herein as 2D.

3D image in three dimensions is perceptible. To understand this, you must know how people will be treated as an object a three-dimensional object. Since the four kinds of physiological factors outlined below, relate to the human visual three-dimensional effect.

- Binocular parallax.
- Accommodation
- Vergence
- Motion parallax

Binocular parallax refers to the difference in position of an object when viewed by the left eye and the right eye separately. When the object is close to the eye, the difference is large, and when the object is far away, the difference is small. Like a camera, the eye has a lens known as the crystalline lens. The eye focuses by changing the lens thickness via an operation known as accommodation. The closer an object is, the more the eyes need to rotate toward each other to focus. The muscle tension involved in this rotation is called vergence, and provides information on the depth of the object. Motion parallax involves the perceived movement of moving objects or that of stationary objects viewed while the observer is in motion. When the viewer

is moving, for example, objects farther away appear to move less than those that are closer.

1.1.2 Current three dimensional display technologies

Current 3D display technologies can be roughly classified into two types, one is a multiple parallax system based on light rays, and the other is a light wave based holography system.

The dedicated devices are need for the multiple parallax system based on light rays. Since they can be implemented relatively easily technically. And they are already widely used in movies, magazines, etc. It is also expected that the market will expand from these viewers There is a problem that the viewpoint is confined only to a fixed or horizontal direction, and only physiological factors for perceiving three dimensional images are satisfied with binocular disparity, so a mismatch between congestion and focal point adjustment , It causes perception of a three-dimensional image unnatural for human beings, and may feel fatigue when watching for a long time

Holography is an ideal display technology [6] to meet all humans' requirements of physical and perception [6] [7] [8] [9]. Holography can record and reconstruct three-dimensional images by using the diffraction and interference principles of object light. A medium for recording the information is called a hologram, and various forms, various hologram forms are available by using a medium. Many holograms are exhibited as art objects, but many of them are still images. Nowadays, using a computer, hologram data can simulate the interference patterns of holograms, which are called computer-generated holograms (CGHs). In addition, an electro-holographic display

device with spatial light modulator (SLM) can display the holographic animations.

1.2 Background of this thesis

Nowadays, visualizing volume data is an important requirement. There are several CG technologies to visualize the volume data. And CG visualization methods for volume data are widely used in medical imaging and geographic imaging. However, these CG technologies cannot satisfy all physiological and perceptual requirements of humans. A CG visualized result is the projection to the imaging plane. It was not real 3D. As we have said, holography is an ideal 3D display technology. Therefore, holographic display methods for volume data is a valuable research topic. And several holographic display methods for volume data have been proposed to generate holograms. For example, the Voxgram system proposed by S. Heart et al. has been a great success in medical imaging [10] [11]. It proved that holograms can be used in medical science and are better than conventional 3D medical-display methods. The hologram is recorded on a photographic plate as a 3D image created by multiple exposures of each equal depth layer of volume data. Holoxica [12] also proposed a holographic display system for medical images. They aimed to visualize the medical data by digital holography. And customers can customize on their website. Y. Sakamoto proposed a volume rendering method [13] that can generate CGHs from volume data. All these method can generate holograms well. And their reconstructed images were 3D. However, they were still images that display as photographic plates and films. And the calculation time is very long. They may cost hours or even tens of hours to calculate the holograms for volume data.

Current CG visualizing methods are not the ideal methods. Therefore, Voxgram system has proved that holographic display method is better than CG display for medical data. There are many shortcomings in the current holographic visualization methods for volume data, such as long calculation time and can not generate holographic animations.

1.3 Purposes of this study

In order to visualize volume data better, I did research about holographic display method for volume data. In my study, holographic animation and viewpoint movement are possible to be realized by using an electro-holographic display. And I have proposed three CGH calculation methods for volume data [14] [15], which can generate holograms with fast enough calculation speed.

In this thesis, I introduce three CGH calculation methods for volume data: polygon-based method, MIP-based method, and volume rendering based method. The polygon-based method can generate colorful holograms, but the MIP-based method just can generate the single color holograms. MIP-based method is much faster than polygon-based method. Both these two methods are able to generate the holographic animations. Volume rendering based method gets the best display effect. However, the calculation amount of volume rendering based method is very large. To improve the speed of calculation, I propose an element holograms based CGH calculation method.

By using these three CGH calculation methods, volume data are able to be visualized. And the effect in stereo vision is better than conventional CG methods. In the future, these CGH calculation methods may be applied to display volume data, espe-

cially medical diagnosis, meteorological and geographic data presentation.

1.4 Structure of this thesis

This thesis consist of 9 chapters. Chapter 1 introduces the background an purpose of this thesis. Chapter 2 talks about the volume data in detail, especially the visualization methods of volume data. Chapter 3 introduces the principle of holography and the CGH calculation methods. Chapter 4 introduce the Fourier transform optical system which was used to enlarge the visual field of holographic device. Chapter 5 introduces the polygon-based CGH calculation method for volume data in detail. In polygon-based method, I first extract the iso-surface of volume data with marching cubes algorithm. And I applied the ray tracing CGH calculation method to generate the holograms for extracted surfaces. Chapter 6 introduces the MIP-based CGH calculation method for volume data in detail. In MIP-based method, I applied a modified ray tracing method and point light based CGH calculation method to generate the MIP holograms of volume data. Chapter 7 introduces the volume rendering based CGH calculation method in detail. In volume rendering based method, I assumes that the reflection model of volume data is the diffuse reflection. And I introduce the volume rendering based method and volume rendering based method with elemental holograms in detail. Chapter 8 is the discussion. Chapter 9 is the conclusion.

2

Volume data

Volume data is 3D data representing, for example, the temporal evolution of a grid spectrum or image. Therefore, depending on the point of view, they can be thought of as a pile of images of the same size or a set of curves forming a regular grid (image). Volume data are generated by a number of experimental methods, including X-ray crystallography, electron microscopy, an so on. In electron microscopy, volumes rep-

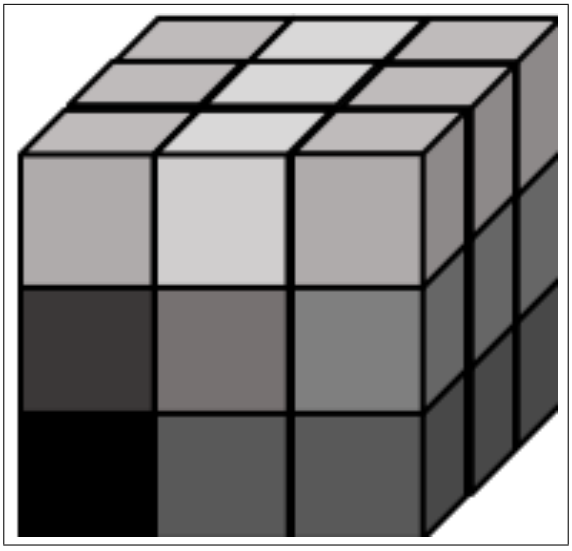

Fig. 2.1 The composition of the volume data.

resenting the electron potential of the sample molecule are reconstructed from many 2D projections extracted from micro-graphs. In crystallography, solution of the phase problem gives electron density maps; which are then invariably interpreted in terms of atomic models.

In this chapter, I will briefly introduce the volume data. In section 2.1, I will introduce the voxel, which was the element of volume data. In section 2.2, I will introduce the uses of volume data. In section 2.3, I will introduce several visualization technologies for volume data.

2.1 Voxel

Volume data values are recorded as voxels on a discrete grid in 3D space, as shown in Fig.2.1.

A voxel is a volume element representing a value on a regular grid in 3D space.

info

1x1 struct 包含 118 个字段

字段	值
Filename	'/Users/lzx/Documents/MATLAB/VolumeRendering4CGH/testdata/IM-0001-0022.dcm'
FileModDate	'19-Oct-2009 11:59:08'
FileSize	53534
Format	'DICOM'
FormatVersion	3
Width	384
Height	384
BitDepth	12
ColorType	'grayscale'
FileMetaInformationGroupLength	204
FileMetaInformationVersion	[0;1]
MediaStorageSOPClassUID	'1.2.840.10008.5.1.4.1.1.4'
MediaStorageSOPInstanceUID	'1.3.12.2.1107.5.2.31.30222.30000006100606325120300005152'
TransferSyntaxUID	'1.2.840.10008.1.2.4.91'
ImplementationClassUID	'1.3.6.1.4.1.19291.2.1'
ImplementationVersionName	'OSIRIX001'
SourceApplicationEntityTitle	'OsiriX'
SpecificCharacterSet	'ISO_IR 100'
ImageType	'ORIGINAL\PRIMARY\M\DIS2D\SUB'
SOPClassUID	'1.2.840.10008.5.1.4.1.1.4'
SOPInstanceUID	'1.3.12.2.1107.5.2.31.30222.30000006100606325120300005152'
StudyDate	'20061006'
SeriesDate	'20061006'

Fig. 2.2 Dicom structure example.

This is similar to a pixel, which represents two-dimensional (2D) image data in a bitmap. It is noted that the voxel is not explicitly encoded together with the coordinate values thereof. Instead, the rendering system based on its position relative to other voxels to infer voxel coordinates. And volume data are stored as a series of DICOM files, which are files capable of recording a variety of information.

Digital imaging and communications in medicine (DICOM) is the standard for the communication and management of medical imaging information and related data [16]. The value of a DICOM file may represent various properties as shown in Fig. 2.2. DICOM files are able to be converted to 2D images. Every DICOM file can be treated as a image. There are several softwares [17] [18] can read the DICOM file as 2D image. And we also can read DICOM files with libraries [19] [20]. In our study, I apply the Matlab [21] to process the DICOM files, which can read the DICOM files with simple functions as follow.

```
dicom = dicomread(filepath);
info = dicominfo (filepath);
```

Function “dicomread” can read the DICOM file as an uint16 image and function “dicominfo” returns the DICOM file information as shown in Fig. 2.2.

2.2 Uses of volume data

Common use of volume data is volumetric imaging in medicine, like CT and MRI. In medical imaging area, CT and MRI data are volume data that record patient information and image information to DICOM files.

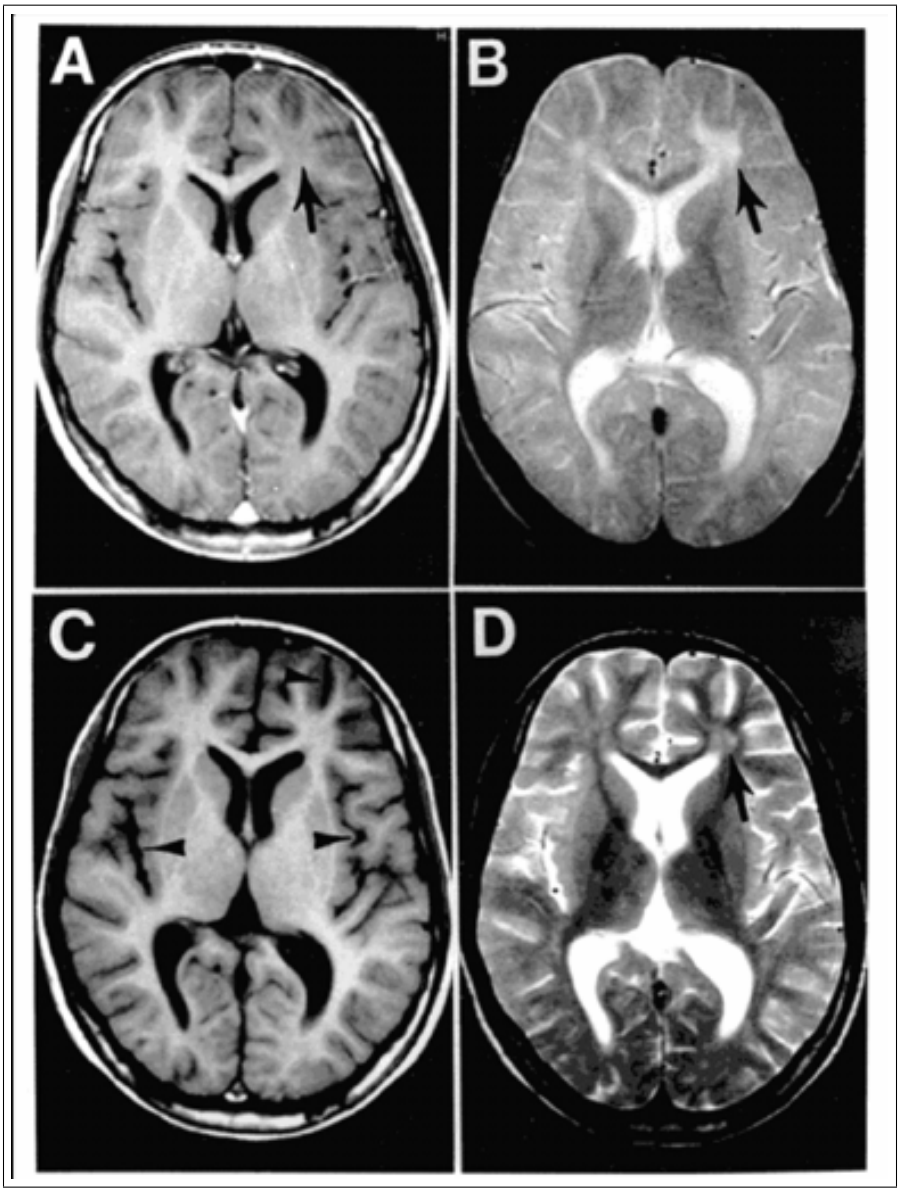

Fig. 2.3 Medical images.

Nowadays, volume data are also widely used in geology area, like representation of terrain and cloud. Voxel terrain is used instead of a height-map because of its ability to represent overhangs, caves, arches, and other 3D terrain features. These concave features cannot be represented in a height-map due to only the top layer of data being represented, leaving everything below it filled (the volume that would otherwise be the inside of the caves, or the underside of arches or overhangs). And voxels are also used in game scenes. In addition, voxels are also used in toy manufacturing.

2.3 Visualization technologies for volume data

To make volume data easy to understand, many excellent visualization technologies have been proposed in the computer graphics (CG) area, such as surface extraction [2], maximum intensity projection (MIP) [3], and volume rendering [4] [5]. In this section, I will introduce the visualization technologies for volume data in detail.

2.3.1 Slice-based method

This is the most straight-forward solution, which implies the separate visualization of every slice of the volume dataset with an opportunity to scroll them interactively.

The simplicity of the implementation and low computational complexity are the key advantages of the technique. However, its main problem is that the viewers should use their imagination to reconstruct an entire object structure. As the result, the slice-based method is not the most suitable for visual analyses of very complex and unknown structures. But it suits well for the detection of features inside the well-known objects, such as parts of human body. That is why the methodology is widely used in

medicine. For example, it is the most popular way of representation for MRI and CT. It is worth to mention, that general CT and MRI studies have much lower resolution in one of the dimensions, which causes some difficulties for utilizing the datasets with more advanced technologies.

2.3.2 Surface rendering

Visualization of 3D object as a 2D image is called 3D rendering. The most common way of the 3D rendering is based on photo-realistic visualization of surfaces which are represented by polygonal meshes. The technology is utilized so widely that modern graphic card's architecture is designed to accelerate the operation.

The main processing of this approach is extracting iso-surface out of a dataset in accordance with certain threshold. There are several algorithms exist to perform the task. The most popular one is Marching Cubes [22]. Sometimes iso-surface extraction can be improved by developing the special algorithm which is based on a specific feature of the particular dataset. Then the polygonal surface model can be visualized by any 3D engine or other tools for visualization of polygonal mesh models

Polygonal models can be edited by 3D softwares, like 3Ds max [23], Meshlab [24] , blender[25], and so on. Based on the editing of polygonal models of volume data, various models can be visualized. The main advantages of this approach are inherited from other technologies. It contains all the typical features of 3D object visualization such as rotation, usage of different amounts of light sources, interaction with other 3D objects and so on. As the result, it makes complex 3D structures analysis much simpler.

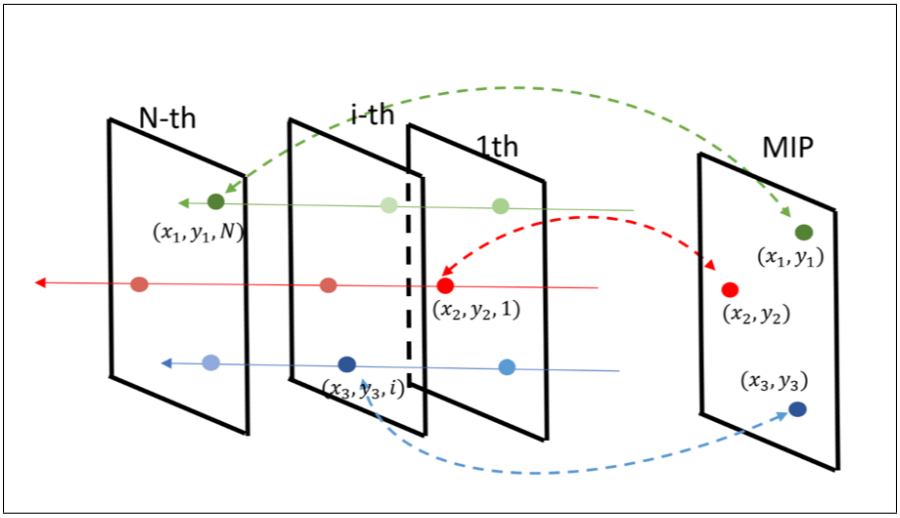

Fig. 2.4 Maximum intensity projection.

2.3.3 Maximum intensity projection

Maximum intensity projection (MIP) is the simplest volume rendering method for volume data. The MIP projects the voxels with the maximum voxel values in the visualization plane, which falls on the orbit of the parallel rays from the viewpoint to the projection plane as shown in Fig. 2.4. MIP is widely used in medical diagnostics to obtain high-intensity objects such as blood vessels and bones. MIP can be calculated quickly. However, MIP cannot provide a good sense of depth of raw volume data. To improve the sense of depth, I reconstruct the MIP data with depth coordinates on the basis of the positions relative to other voxels. In one view direction, only one MIP result can be obtained. Usually, MIP result is a single color image.

2.3.4 Direct volume rendering

Surface rendering is an indirect volume rendering method. There are two steps in surface rendering, surface extraction and model display. Different with indirect volume rendering method, direct volume rendering method does not require any preprocessing. The volume data is visualized from an original dataset. It gives the algorithms an opportunity to modify the transfer function and threshold dynamically. Also, some of the approaches allow to visualize the internal structure of the dataset in semi-transparent way.

There are several different technological implementations of direct volume rendering. The most common of them use the tools created for a GPU acceleration of polygonal mesh models rendering in their own way. Texture-based volume and volume ray casting are presently the most successful approaches of direct volume rendering. Texture-based volume rendering approach uses a set of planes to construct the object. The dataset is projected to the planes as textures. The final picture is combined by alpha blending of the planes. Volume ray casting approach uses cube as a placeholder for the volume model. The model itself is projected to the sides of the cube by the ray casting algorithm which uses rays to accumulate the data and combine it with the specific equation called Ray function. Ray function is truly fascinating feature of volume ray casting. It allows to define how rays perform sampling of the dataset and calculation of the pixel color.

2.3.5 Holographic display methods for volume data

Holography is an ideal display technology [6] that can satisfy all physiological and perceptual requirements of humans [6] [7] [8] [9]. Several holographic display methods have been proposed to generate holograms that represent volume data.

The Voxgram system proposed by S. Heart et al. achieved great success in medical imaging [10] [11] .It proved that the hologram can be used in medical science, and the method is better than the traditional display of medical images. The hologram recorded as a 3D image is generated by multiple exposures of each of an equal volume of depth data layers in the photographic plate.

Holoxica [12] also proposed a holographic display system for medical images. They offer custom digital hologram design services to customers in medical imaging, scientific visualization and engineering design. They can convert the data into full color 3D holograms using advanced holographic printing technology. And it usually takes a couple of weeks to turn a design around: around 5-10 days for design and allow 10-15 days for manufacturing on the holoprinter. In addition, Y. Sakamoto proposed a volume rendering method [13] that can generate CGHs from volume data. The reconstructed images of these methods were 3D images, but they were still images that display as photographic plates and films.

3

Holography

Holography was invented by Hungarian physicist Dennis Gabor in 1948 [7]. At that time, Gabor proposed a method to record the phase as interference fringes by using light interference. The one on which the interference fringes are recorded is a hologram.

There are several important characteristics for holography. First, it is possible to

reconstruct a complete 3D image; second, it is possible to multiplex recording; third, it can convert the wavefront; fourth, a light source with good coherence is necessary; fifth, high resolution recording material is required.

In this chapter, I will introduce the holography from following aspects : section 3.1 will introduce the principle of holography, section 3.2 will introduce the computer generated hologram in detail, and section 3.3 will introduce the electro-holography.

3.1 Principle of holography

Holography was firstly invented by Gabor [7]. However, the currently widely accepted holographic theory was proposed by Leith [6]. There are two main parts: recording of holography and reconstituting of holography. In this section, I will introduce them in detail.

3.1.1 Recording of holography

In holography, for each point, the phase of the light wave is recorded using the reference light. The reference light comes from the same light source as the object illumination light that illuminates the object to be recorded. Object light and reference light are coherence lights. Interference fringes are formed by interference of light by superposition of the reference light and the object light. This is the same as shooting technique with ordinary photographic film, but since it is necessary to record a fine image of interference fringes, it is common to use a dedicated film and use an anti-vibration table. These interference fringes form a diffraction grating on the film.

In order to understand the principle of recording easily, I gave a figure to show it as

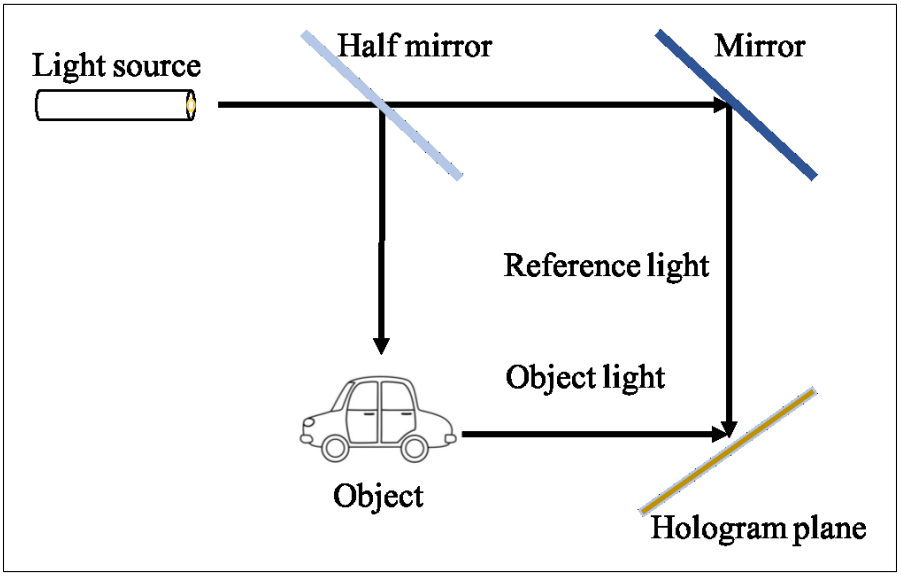

Fig. 3.1 Recording of holography.

Fig. 3.1. The beam emits from the light source, which can be the laser light or LED light. The beam is split into two beams by half mirror. One of the beams is reflected by the object, and the reflected light is called object light. Another beam is treated as reference light. Interference fringes are formed by interference of the reference light and the object light. The interference fringes are recorded on the hologram plane.

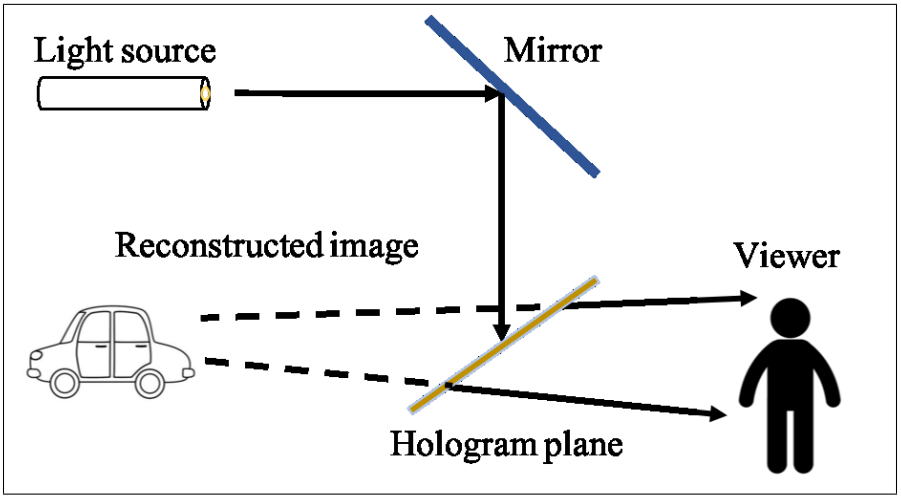

Fig. 3.2 Reconstructing of holography.

3.1.2 Reconstructing of holography

Once the interference fringes were recorded on holograms, the object can be reconstructed when the reference light is irradiated again. And the object light reproducing light intensity and phase is generated. Since the light intensity and phase are reproduced, the image is 3D.

In order to understand the principle of reconstructing easily, I gave a figure to show it as Fig. 3.2.

3.2 Computer generated holograms

The principle of holography is as shown in section 3.1. However, there are several difficulties for original holograms. In this section, I will introduce the computer generated holograms (CGHs) in detail . CGHs are generated by simulating the recording process in holography by a computer. Specifically, it is necessary to calculate the light from the object and the reference light, and their interference fringes.

3.2.1 The advantages of CGHs

Due to object light, reference light, and interference fringes are calculated on the computer. There are several advantages of CGHs.

- There is no need to design the optical system. In the usual recording process, since the position of the object, the light source, the recording material, the half mirror, etc. and the angle of incidence of the light are manually set, there is a disadvantage that it takes much time and effort for fine measurements.
- Avoiding dangerous of making the holograms. Various chemicals are used for recording materials in ordinary holograms, and some of them may contain dangerous chemicals.
- It is easy to obtain recording material. There is also a problem that ordinary holograms can not actually obtain high-resolution recording materials because chemicals to be used currently have prohibited use of chemicals themselves. In computer generated holograms, it is possible to display on high resolution

liquid crystals or on things like OHP film, so you can make hologram relatively easily.

As described above, computer-generated holograms are attracting attention because they perform their recording process on a computer, eliminating labor and cost of actually preparing and installing optical instruments, and avoiding danger in work. Of course, like the usual holography technology, object light can be perfectly reproduced, and ideal three-dimensional display satisfying all human visual functions is possible.

3.2.2 The flow of CGH calculation

There are three parts of CGH calculation, input object data, calculate the propagation of object light and reference light, and calculate the interference pattern as shown in Fig. 3.3.

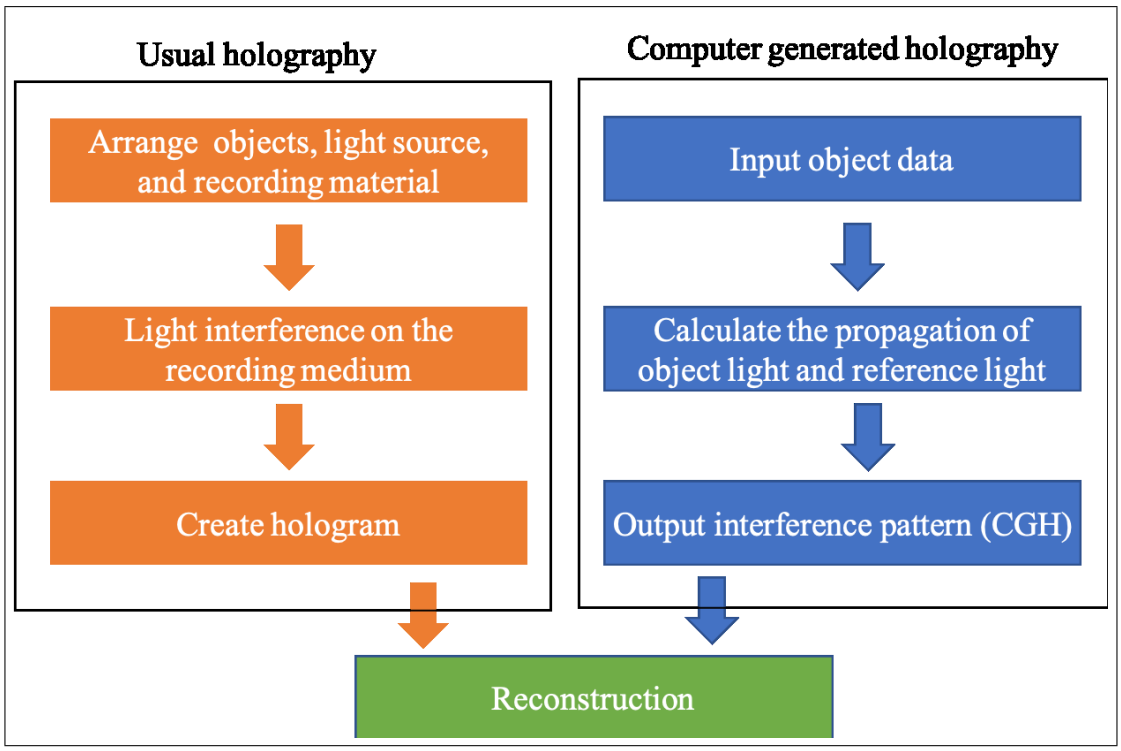

Fig. 3.3 The flow of CGH.

First of all, input the data of the object you want to create in the computer. The input data may be a plane object or coordinate data of a set of points. Next, set the distance to be propagated and calculate the wave propagation of the object assuming that there is a recording plane at that position. Finally, output the intensity of the complex amplitude distribution obtained on the recording plane to the file is CGH.

Compared with the usual holography, these steps are calculated on a computer.

3.2.3 CGH calculation

The CGH calculation includes three parts: object light calculation, reference light calculation, and interference pattern calculation.

The Fresnel-Kirchhoff diffraction integral formula is used to calculate object light. It is calculated by

$$\mu(\xi, \eta) = \frac{j}{\lambda} \int \int \int_{-\infty}^{+\infty} g(x, y, z) \frac{e^{-jkr}}{r} dxdydz, \tag{3.1}$$

where $\mu(\xi, \eta)$ is the object light observed on the hologram plane, $g(x, y, z)$ is the object distribution, k is the wave number, r is the distance between the object and hologram plane. In addition, $k = 2\pi/\lambda$, λ is the wavelength. Based on this equation, there are two CGH computational techniques: the point light based method and Fourier transform-based method.

In CGH calculation, a point light source and a plane wave are extensively used as reference light. This section outlines a plane wave based on simple calculation. If the incidence of reference light is perpendicular to the hologram, the reconstructed image will be hard to see. It is therefore desirable to ensure that the light falls on the holo-

gram at a certain angle. When reference light is inclined at ϑ to the axis η, its phase distribution on the hologram $\varphi(\eta)$ is calculated as

$$\varphi(\eta) = exp(jk\eta sin\vartheta). \tag{3.2}$$

In this case, the amplitude of the reference light is considered to have a certain value. This value can be freely set, but if the light relative to the object is too strong or too light, a light impact where the light is too strong on the other, resulting in interference fringes difference. As an example, let us consider a case where the maximum value of the complex amplitude of the object light between the points on the hologram is used as the amplitude of the reference light. In this case, the distribution of the reference light on the hologram plane $R(\xi, \eta)$ is calculated by

$$R(\xi, \eta) = max(|\mu(\xi, \eta)|)exp(jk\eta sin\vartheta). \tag{3.3}$$

The interference pattern can be determined by calculating the interference between the object light and the reference light obtained as described above. The intensity distribution of the interference pattern $I(\xi, \eta)$ is calculated by

$$I(\xi, \eta) = |\mu(\xi, \eta) + R(\xi, \eta)|^2. \tag{3.4}$$

3.2.4 Point light based method

The point light based method is a commonly used method for CGH calculating. In this method, an object is treated as a point light cloud as shown in Fig. 3.4. Each

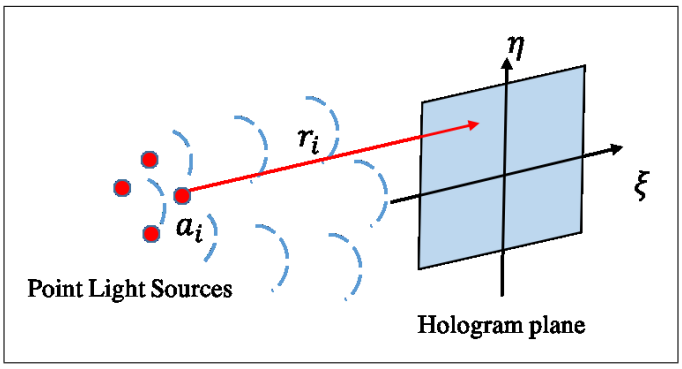

Fig. 3.4 Point light based CGH calculation method.

point is a point light. This method can express objects of any shape. However, computation time is enormous which was in proportion to the number of points. Due to the development of graphics processing units (GPUs) and dedicated hardware, as well as parallel computing and other methods, the recent computational time has been alleviated.

For point light i, the complex amplitude of the point light source on the hologram plane is calculated by

$$\mu_i(\xi, \eta) = \frac{a_i}{r_i} exp(-j(kr_i + \varphi_i)), \tag{3.5}$$

where a_i is the amplitude of point light i, φ_i is the phase of point light i. r_i is the distance between the point source i and the pixel on the hologram plane (ξ, η), and it is calculated by

$$r_i = \sqrt{(\xi - x_i)^2 + (\eta - y_i)^2 + z_i^2}. \tag{3.6}$$

Accordingly, if the number of point sources making up the object is denoted by N,

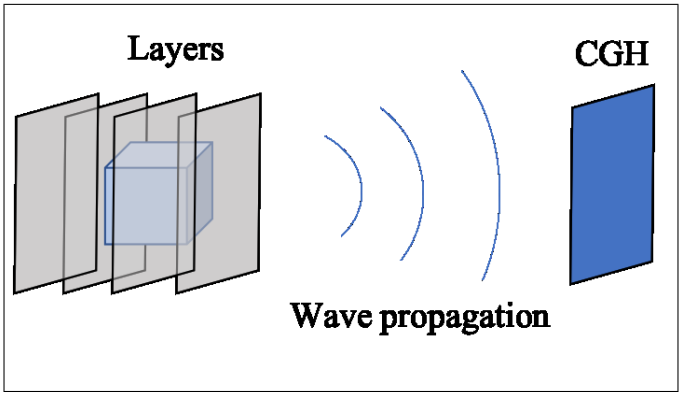

Fig. 3.5 Fourier transforms-based CGH calculation method.

the light from the entire object $\mu(\xi, \eta)$ is calculated by

$$\mu(\xi, \eta) = \sum_{i=1}^{N} \mu_i(\xi, \eta). \tag{3.7}$$

3.2.5 Fourier transforms-based methods

Fourier transforms-based methods involve the use of Fourier transforms with the input object limited to its plane parallel to the hologram plane. CGHs can be calculated with high speed by use the fast Fourier transforms (FFT). However, the input data type is limited.

Recently, a method of inputting a plane which is not parallel with the hologram plane has been proposed, and display of complicated objects is also becoming possible. There are usually three methods involved in using the Fourier transform: Fresnel diffraction based, Fraunhofer diffraction based, and angular spectra based methods.

3.2.5.1 Fresnel diffraction based method

In this method, r is approximate calculated by quadratic formula as

$$\begin{aligned} r &= \sqrt{(\xi - x)^2 + (\eta - y)^2 + z_o^2} \\ &\approx \frac{(\xi - x)^2}{2z_o} + \frac{(\eta - y)^2}{2z_o} + z_o \\ &= \frac{\xi^2 + x^2}{2z_o} - \frac{\xi x + \eta y}{z_o} + \frac{x^2 + y^2}{2z_o} + z_o, \end{aligned} \tag{3.8}$$

where z_o is the distance between the object surface and the hologram plane.

Substituting Eq. 3.8 into the diffraction integral of Fresnel-Kirchhoff, the new equation can be obtained as

$$\begin{aligned} \mu(\xi, \eta) &= \frac{j}{\lambda z_o} exp(-jkz_o) \int\int_{-\infty}^{+\infty} g(x, y) p(\xi - x, \eta - y) dxdy \\ &= const\{g(\xi, \eta) p(\xi, \eta)\}, \end{aligned} \tag{3.9}$$

where $p(\xi, \eta)$ is a transfer function defined as

$$p(\xi, \eta) = exp(-j\frac{k}{2z_o}(\xi^2 + \eta^2)). \tag{3.10}$$

Since convolution integration can be calculated at high speed using FFT, high-speed object light calculation can be realized.

3.2.5.2 Fraunhofer diffraction based method

In this method, the r is approximate calculated by

$$r \approx \frac{\xi^2 + \eta^2}{2z_0} - \frac{\xi x + \eta y}{z_0} + z_0, \tag{3.11}$$

where z_0 is the distance between the object surface and the hologram plane.

Same with Fresnel diffraction based method, substituting Eq. 3.11 into the diffraction integral of Fresnel-Kirchhoff, the new equation can be obtained as

$$\begin{aligned} \mu(\xi, \eta) &= \frac{j}{\lambda z_0} exp(-jk\frac{\xi^2 + \eta^2}{2z_0}) \int\int_{-\infty}^{+\infty} g(x, y) exp(j\frac{k}{z_0}(\xi x + \eta y)) dxdy \\ &= const F^{-1}(g(x, y)), \end{aligned} \tag{3.12}$$

where F^{-1} is the function of inverse Fourier transform.

In this way, Fraunhofer diffraction can be expressed in the form of Fourier inverse transform, so fast calculation can be performed using FFT.

3.2.5.3 Angular spectra based methods

In this method, the object light is calculated by the following processes:

- Converting the pre-propagating light waves on the plane into plane waves.
- Calculating the propagation of each plane wave.
- Superimposing results onto the planar surface after wave propagation.

These processes can be represented by the following formulas,

$$G(f(\xi), f(\eta)) = \int\int_{-\infty}^{+\infty} g(x, y) exp(-2\pi j(xf(\xi) + yf(\eta)))dxdy, \tag{3.13}$$

$$U(f(\xi), f(\eta)) = G(f(\xi), f(\eta)) exp(-2\pi jf(z)z_0), \tag{3.14}$$

$$\mu(\xi, \eta) = \int\int_{-\infty}^{+\infty} U(f(\xi), f(\eta)) exp(2\pi j(\xi f(\xi) + \eta f(\eta)))df(\xi)df(\eta), \tag{3.15}$$

where $f(z)$ is a spatial frequency component along the z axis defined as

$$f(z) = \sqrt{\frac{1}{\lambda^2} - f(\xi)^2 - f(\eta)^2}. \tag{3.16}$$

First and third procedures can be processed using a Fourier transform and an inverse Fourier transform, respectively. The second procedure also requires little computation time. Accordingly, the method enables high-speed overall calculation.

3.2.6 Previous CGH calculation methods

In previous sections, I have introduced the basic CGH calculation approaches. And there are several disadvantages. The calculation time of CGH is too long. It is always an important disadvantage. And there is no rendering method for CGH. In order to solve these two problems, several advanced CGH calculation methods have been proposed.

Currently, the calculation speed was increasing with GPUs. And the nvidia com-

pany [26] proposed the most accelerated computing toolkit, which was called compute unified device architecture (CUDA). And CGH calculation methods with GPUs have increased a lot of speed [27] [28]. And many algorithms have been proposed to increase the calculation speed. The look-up table CGH calculation method [29] is a very famous method. And a series of variant look-up table based CGH calculation methods have been proposed [30] [31] [32]. Ogihara [33] and Sugawara [34] have proposed CGH calculation methods for polygonal models with point light based method. And their methods have obtain great progress.

Rendering for CGH calculation is a difficult. And many CGH calculation methods with rendering methods have been proposed. For example, Wakunami [35] and Ichikawa [36] used the ray tracing methods to do the rendering for CGH calculation. Matsushima [37] proposed a CGH calculation method for 3D surface with shade and texture. In these methods, hidden surface removal and shadings are realized. The reconstructed images are more realistic than before. Watanabe [38] has proposed a fast holographic animation generated method with ray tracing method. His method aimed to increase the calculation speed of holographic animation, which was several times faster than calculate by frames.

The CGH calculating for real objects is also an important research topic. The objects can be reconstructed by CG reconstructed methods or 3D scanner. Lee [39] and Chang [40] have proposed their own CGH calculation method for real object. These methods can be used in holo-TV in future.

3.3 Electro-holography

Traditional holograms are still images. In order to display holographic animations, the electro-holography was proposed. By using the spatial light modulator (SLM), the objects recorded on interference patterns can be reconstructed. Generally, an electro-holographic display includes a SLM, a light source, lenses, and mirrors. Many electro-holographic displays have been proposed. They have different features. They have different viewing zones and visual field. They may be single color or RGB full color displays.

In this thesis, I applied an eyepiece -type electro-holographic device, which has been proposed by Yoneyama [41] in 2013. In this system, the light source is the white LED. And the viewing angle is 8 degrees. Currently, there are several 360 degree electro-holographic displays [42] [43] [44] [45] have been proposed. They obtained great success and the reconstructed images were amazing.

In another research direction of electro-holography, the head mounted displays (HMDs) for electro-holography received the attention of researches. Murakami [46] has proposed a compact holographic HMD for augmented reality (AR). It reconstructed the objects in AR mode successfully. However, this display is single color display. And microsoft also proposed a holographic HMD [47]. This holographic HMD presents novel designs for virtual and augmented reality near-eye displays based on phase-only holographic projection. And their method is built on the principles of Fresnel holography and double phase amplitude encoding with additional hardware, phase correction factors, and spatial light modulator encodings to achieve

full color, high contrast and low noise holograms with high resolution and true per-pixel focal control. Yoneyama [48] proposed a two eyes holographic HMD with correct accommodation and vergence stimuli. And he proved that the effect of binocular vision is better than that of monocular.

4

Fourier transform optical system

In chapter 3, I have introduced the related contents of holography. And the electro-holography was also discussed in the last section of previous chapter. And the small visual field is a limit for electro-holographic displays. In this chapter, I will introduce a Fourier transform optical system (FTOS) [49], which can enlarge the visual field of electro-holographic displays. Section 4.1 will introduce the components of FTOS.

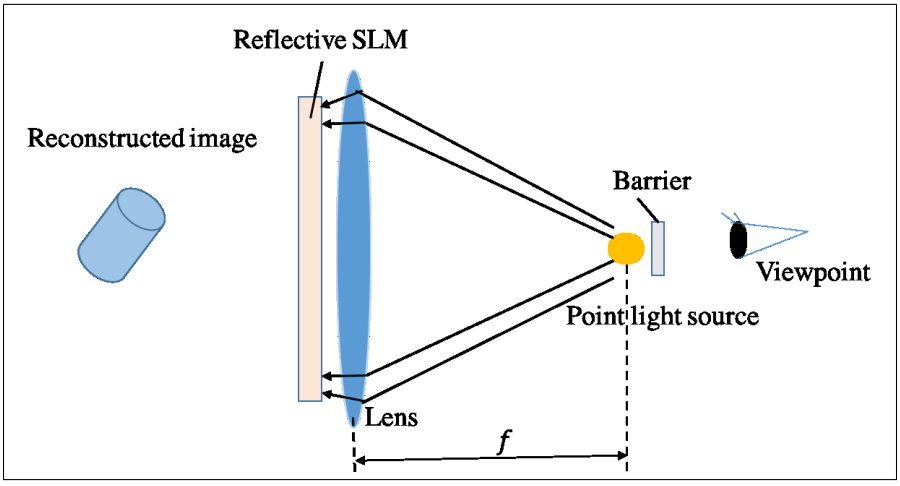

Fig. 4.1 Fourier transform optical system.

Section 4.2 will talk about the compensation calculation for FTOS. Section 4.3 will talk about the point light based CGH calculation method for FTOS.

4.1 Components of FTOS

In oder to enlarge the visual field of electro-holographic display, the FTOS was applied in my research. FTOS was composed of a lens, a reflective SLM, and a point light source as a reference light at the focal point of the lens as shown in Fig. 4.1. The diffraction angle is very small for the original SLM-only optical system. And I can bend the light at the part where a large diffraction angle is required around the viewpoint by using a lens. Therefore, a large viewing angle can be obtained. In addition, unnecessary 0-order light can be cut by providing a barrier at a position where the 0-order light is concentrated.

Figure 4.2 shows that the visual field of FTOS was really expanded. The reconstructed light is converged by the lens, and passes through a window with width w

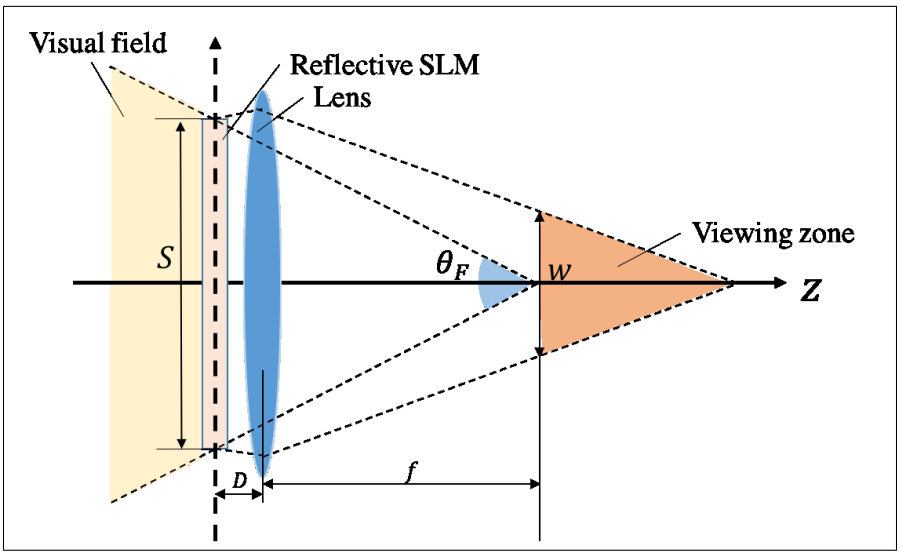

Fig. 4.2 Expanded visual field and viewing zone.

calculated by

$$w = \frac{\lambda f}{p}, \tag{4.1}$$

where p is the pixel pitch of the electro-holographic display. And the viewing angle ϑ_F is calculate by

$$\vartheta_F = 2 \cdot \tan^{-1}\left(\frac{S}{2(f+D)}\right), \tag{4.2}$$

where S is the size of the interference pattern, D is the distance between the reflected SLM and lens.

From Eqs. 4.1 and 4.2, I can know that the viewing angle ϑ_F was increased as the viewing zone became narrow. And the FTOS is suitable for the near eye electro-holographic displays.

4.2 Compensation calculation for FTOS

As last section described, the visual field was expanded by using FTOS. This means that FTOS will cause the shape distortion of the reconstructed image. And the CGH calculation method with FTOS is also different from the conventional CGH calculation method. It is necessary to compensate for the change in coordinate for the FTOS.

The compensation principle is shown in Fig. 4.3. From Fig. 4.3, the lens is at distance D away from the hologram plane, in which the hologram will be enlarged by the lens and form an image at depth z_h . If the coordinates of a virtual object point is (x_i, y_i, z_i), the coordinates of the point light source $(x_i^{'}, y_i^{'}, z_i^{'})$ for CGH calculation will be calculated by

$$z_i^{'} = -\frac{fA}{f - A}, \tag{4.3}$$

$$x_i^{'} = x_i z_i^{'} B, \tag{4.4}$$

$$y_i^{'} = y_i z_i^{'} B, \tag{4.5}$$

where $(x_i^{'}, y_i^{'}, z_i^{'})$ is the coordinate of the point light source i and (x_i, y_i, z_i) is the coordinate of the visual object point i. The A and B in Eqs. 4.3, 4.4, and 4.5 are calculated by

$$A = \frac{z_i(f - D) + D^2}{z_i - D - f}, \tag{4.6}$$

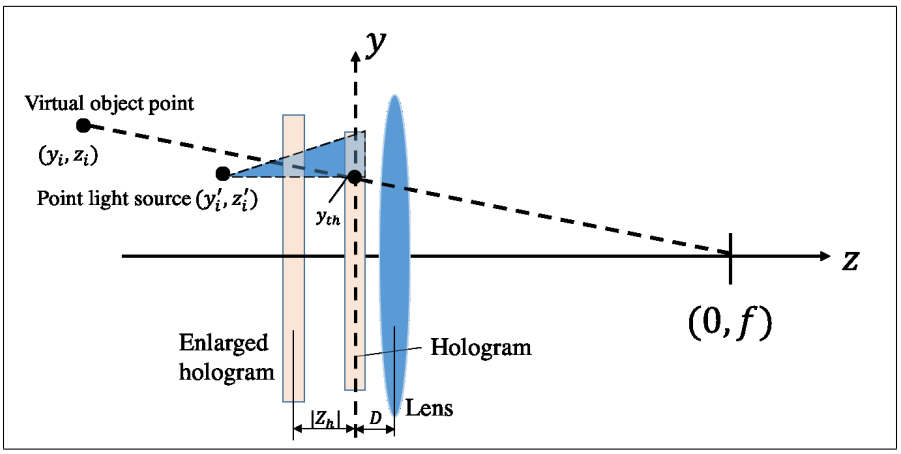

Fig. 4.3 Compensation of reconstructed image.

$$B = \frac{A + D - f}{Af}. \tag{4.7}$$

4.3 Point light-based CGH calculation method for FTOS

In last chapter, I have introduced the CGH calculation method. And I have talked about the point light-based method for object light calculation. However, the coordinates of visual object points are needed to be compensated as last subsection for FTOS. The object light calculation for FTOS was shown as follow.

For point light source i, the light distribution $\mu_i(\xi, \eta)$ is rewritten as

$$\mu_i(\xi, \eta) = \frac{a_i}{r_i} exp(-j(kr_i + \varphi_i)), \tag{4.8}$$

where a_i is the amplitude of point light source i. And φ_i is the random phase of point light source i. $k = 2\pi/\lambda$, where λ is the wavelength of light. r_i is the compensated

distance between point light source i and the pixel (ξ, η) on hologram plane. As last section said, the coordinates of visual object should be compensated. And the equations were listed in last section. When r_i was used to calculate the object light waves on hologram plane, the compensated coordinates should be $(x_i^{'}, y_i^{'}, z_i^{'})$. And r_i is calculated by

$$r_i = \sqrt{(x - x_i^{'})^2 + (y - y_i^{'})^2 + z_i^{'2}}. \tag{4.9}$$

The complex amplitude distributions on the hologram plane were rewritten as

$$\mu(\xi, \eta) = \sum_{i=1}^{N} \mu_i(\xi, \eta), \tag{4.10}$$

where N is the number of point light sources.

5

Polygon-based CGH calculation method

In this chapter, I will introduce polygon-based CGH calculation method for volume data [14]. Section 5.1 will introduce the procedure of polygon-based method. Section 5.2 will introduce the polygon-based CGH calculation method in detail. Section 5.3 will introduce the experiments of polygon-based CGH calculation method.

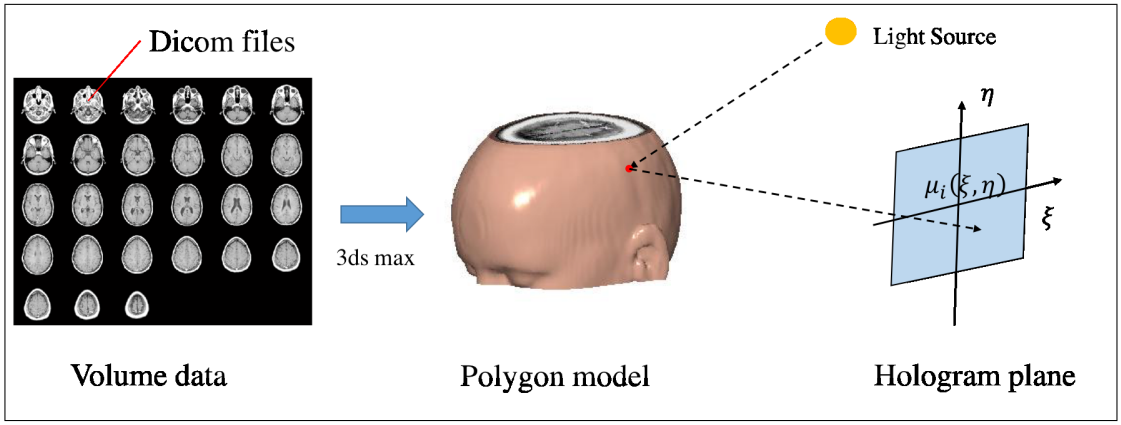

Fig. 5.1 Polygon-based CGH calculation method for volume data.

5.1 Procedures of polygon-based method

The procedures of polygon-based CGH calculation method were shown in Fig. 5.1. There are two operations in polygon-based CGH calculation method, surface extraction of volume data and CGH calculation for polygonal models.

For the first operation, I applied the OsiriX [17] to generate the polygonal models of volume data. And I can edit the models with 3D editing softwares, like 3ds max [23], blender [25], and Meshlab [24].

For the second operation, I use the ray tracing CGH calculation method [50] to generate the holograms for volume data. The ray tracing CGH calculation method can render the polygonal meshes as the Phong reflected model.

5.2 Polygon-based CGH calculation method

In this method, I first generate and edit the polygonal models. And then I applied the ray tracing CGH calculation method [50] to generate the holograms. The principle

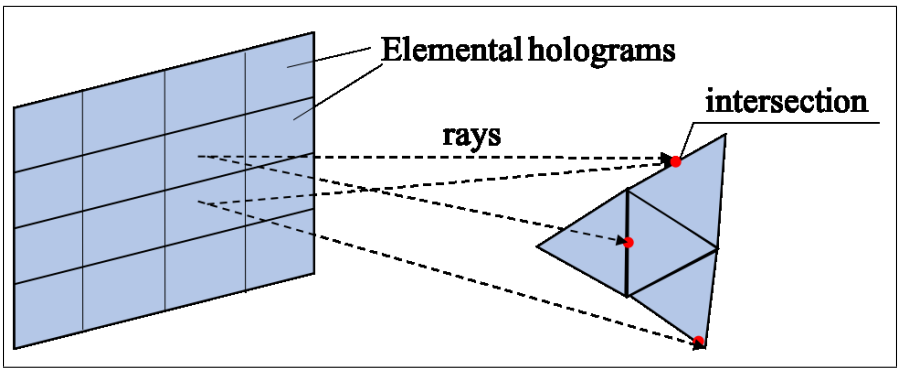

Fig. 5.2 Ray tracing CGH calculation method.

of ray tracing CGH calculation method is shown in Fig. 5.2. The ray emits from the viewpoint to the models. The intersections between the model and rays were treated as the point light sources. In ray tracing CGH calculation method, the polygonal models were treated as the Phong models as shown in Fig. 5.3. And the brightness of intersections were changed by various reflectance distributions. When the diffuse reflection is defined as a Lambert reflection, the intensity of the reflected light is calculated as follows,

$$I_r = I_L k_a + (\mathbf{N} \cdot \mathbf{L}) I_L k_d + I_L k_s (\mathbf{R} \cdot \mathbf{V}) \quad , \tag{5.1}$$

where, I_L is the intensity of light source, k_a, k_d and k_s correspond to the ratio of ambient light, Lambert light and specular light, respectively ($k_d + k_s = 1$). $\mathbf{N}$ is the normal unit vector. $\mathbf{L}$ is the unit vector pointing to the light source. $\mathbf{R}$ is the unit vector of regular reflection direction. And $\mathbf{V}$ is the unit vector pointing to viewpoint. β is the parameter that controls the characteristics of highlight.

After the ray tracing rendering operation, the complex amplitude distributions on the hologram plane would calculated by the point light based CGH calculation

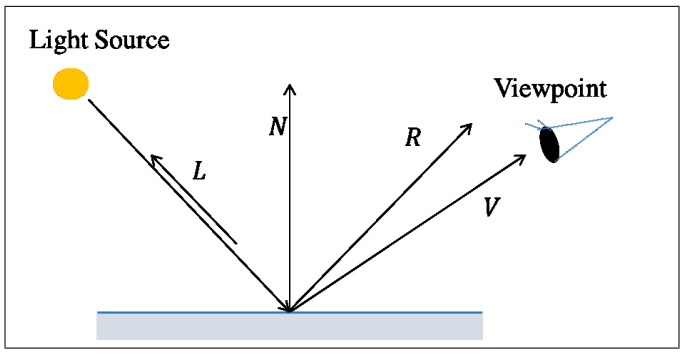

Fig. 5.3 Phong reflection model

method. Eq. 4.8 and Eq. 4.10 should be rewritten as follow:

$$\mu_i(\xi,\eta) = \frac{\sqrt{I_{ri}}}{r_i} exp(-j(kr_i + \varphi_i)), \tag{5.2}$$

$$\mu(\xi,\eta) = \sum_{i=1}^{N} \mu_i(\xi,\eta), \tag{5.3}$$

where $\sqrt{I_{ri}}$ is the amplitude of intersection i. And φ_i is the random phase of intersection i. r_i is the compensated distance between the intersection i and the point on the hologram plane calculated by Eq. 4.9. N is the number of intersections.

5.3 Experiments

5.3.1 Experimental setup

In this chapter, experiments are performed on an electro-holographic display as shown in Fig. 5.4, which was proposed by Yoneyama [41] in 2013. In the display system, a white LED was applied as the light source. And the reconstructed images were col-

orized using the time division method [51]. The illuminated source is emitted through the lens to the SLM and the reconstructed light is reflected by the half mirror. The reconstructed light converges around the observation window. The observer can observe the full-color reconstructed image through the viewing window.

The parameters of the electro-holographic display and the computer are shown in Tables 5.1 and 5.2. In this chapter, I used medical images as experimental data. The experimental dataset includes two parts: the DICOM Image Library [52] and real patient data.

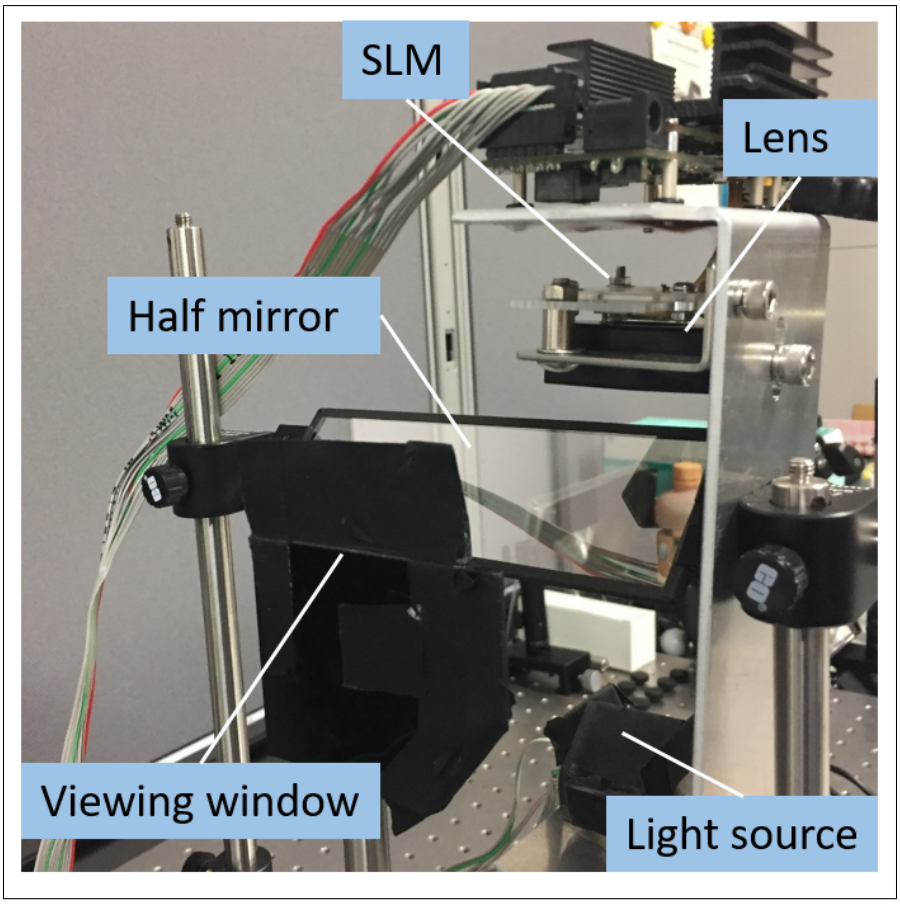

Fig. 5.4 CGH reconstruction device.

Table 5.1 Parameters of electro-holographic display

Pixel pitch of SLM	9.6 x 9.6[μ m]
Number of pixels	1280 x 768[pixels]
Refresh rate of SLM	180 [Hz]
Focal length of lens	100 [mm]
Wavelength of Red	625 [nm]
Wavelength of Green	525 [nm]
Wavelength of Blue	465 [nm]

Table 5.2 Parameters of computer

CPU	i7-6700
Operating system	Ubuntu 14.04 LTS
RAM	8 GB
GPU	GTX TITAN
CUDA	CUDA 8.0

5.3.2 Optical reconstruction

In this subsection, I perform an optical experiment. Figure 5.5 shows the geometry of this experiment. In this experiment, there are two objects: red and green hands. The obj1 is the red hand, and the z coordinate is -30 cm. The obj2 is the green hand, and the z coordinate is -100 cm. I generated the hologram as this geometry. And I captured the reconstructed image in different depth as shown in Fig. 5.6. From Figs. 5.6(a) and 5.6(b), I can know that when the camera was focused on one data, the other appeared blurred. This means that Figs. 5.6(a) and 5.6(b) reconstruct the depth correctly.

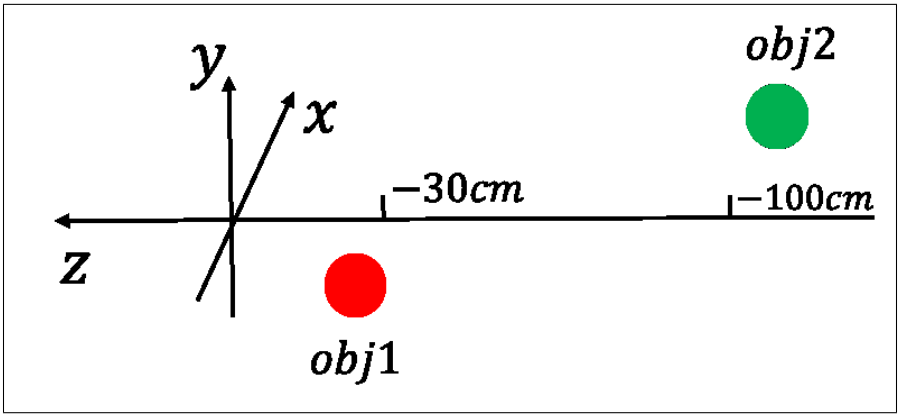

Fig. 5.5 Geometry of parallax experiment.

5.3.3 Reconstructed images

In this subsection, I perform two experiments. First experiment is the reconstruction of head data (data type: CT). The results are shown in Fig. 5.7. In Fig. 5.7, (a) is the CG model and (b) is the reconstructed image. From this figure, I can determined that the polygon-based CGH calculation method can generate hologram for volume data well. And I can see the highlight effect from Fig. 5.7(b).

The second experiment is the CGH calculation of the torso data (data type : CT). As I have said in this chapter, multiple polygonal models can be obtained from the same volume data as shown in Figs. 5.8 (a), 5.8(c), and 5.8(e). And the reconstructed images of polygon-based CGH calculation method are shown in Fig. 5.8. From Fig. 5.8, I determined that the polygon-based CGH calculation method can express the 3D sense of objects well. And the materials of objects can be correctly expressed by the polygon-based method. In next chapter, I will apply torso data to do the experiment of calculation time. And I will compare polygon-based and MIP-based CGH calculation

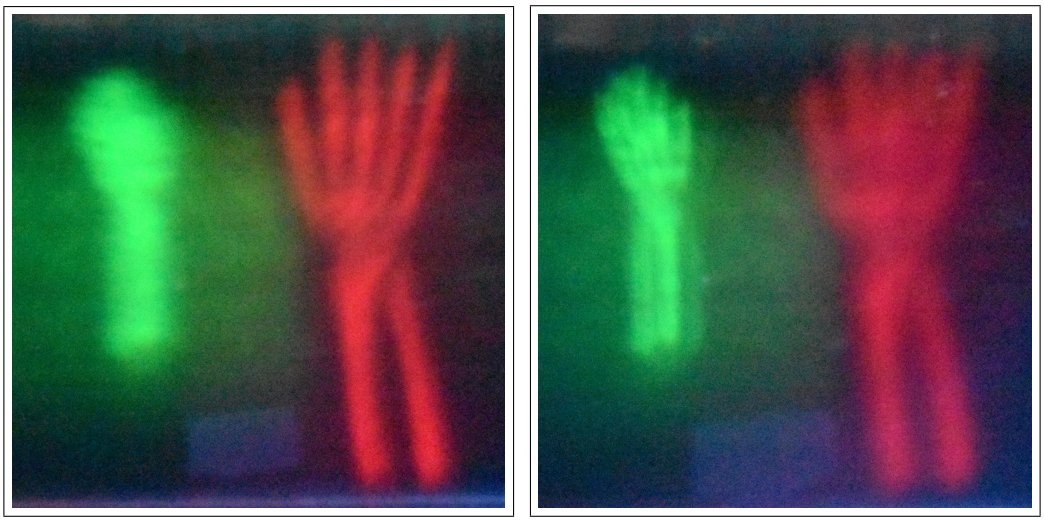

(a) Focusing on obj1. **(b)** Focusing on obj2.

Fig. 5.6 Reconstructed images of different focusing depths.

methods together.

5.3.4 Holographic animation

In this chapter, an electro-holographic display was applied. In Table 5.1, the refresh rate of SLM is 180 Hz. So, holographic animations are able to display on this device. Although the CGH calculation speed with GPU was great increased. Polygon-based CGH calculation method was not able to generate the holograms in real-time. In this subsection, a 36 frames rotation animation of a gallbladder was generated by the polygon-based CGH calculation method.

Several frames generated by the polygon-based CGH calculation method are shown in Fig. 5.9. In the Fig. 5.9, sub-figures (a) and (c) are the reconstructed images from opposite directions. This means the polygon-based CGH calculation method has the

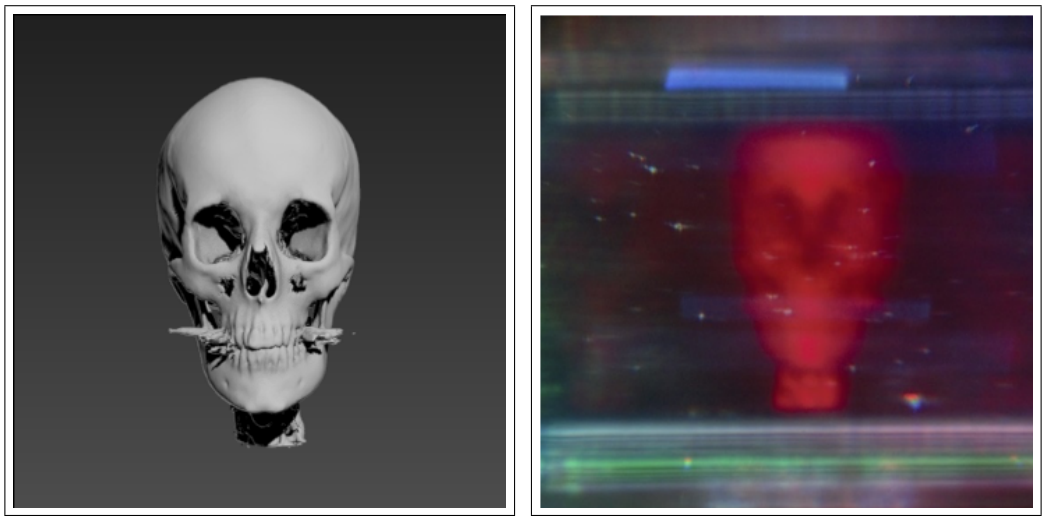

(a) CG model **(b)** Reconstructed image

Fig. 5.7 Reconstructed images of head data.

hidden surface removal processing.

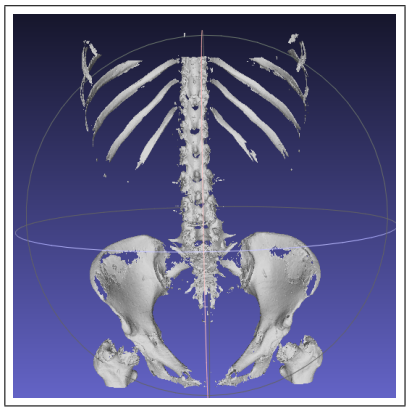

(a) Skeleton

(b) Reconstructed image of skeleton

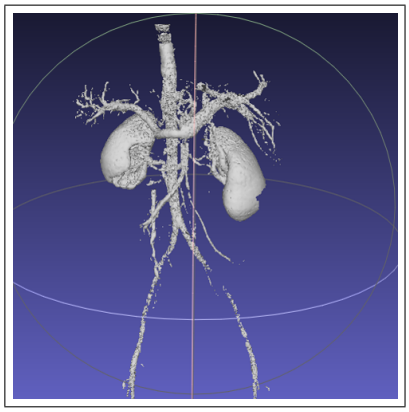

(c) Visceral

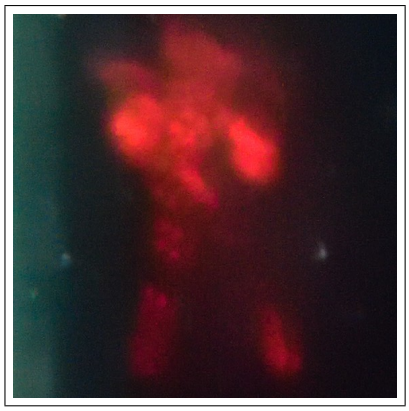

(d) Reconstructed image of visceral

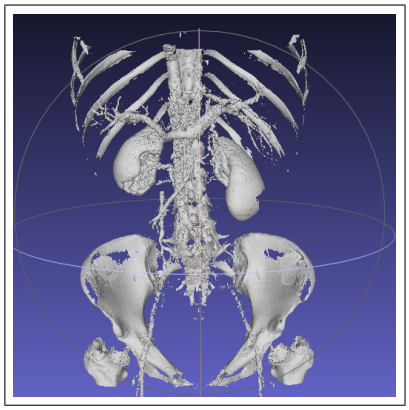

(e) Skeleton and visceral

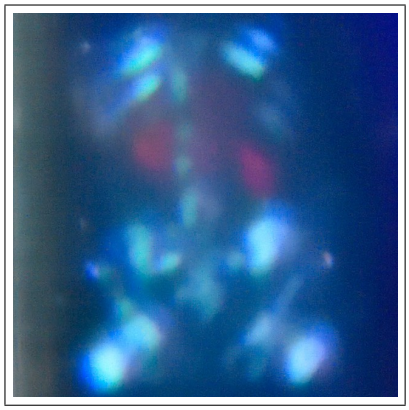

(f) Reconstructed image of skeleton and visceral

Fig. 5.8 Polygon models and reconstructed images of torso

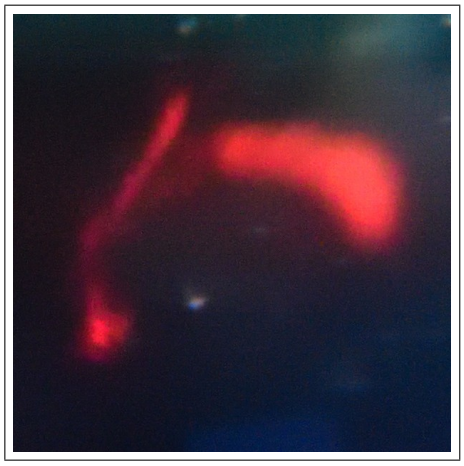

(a) 1st frame

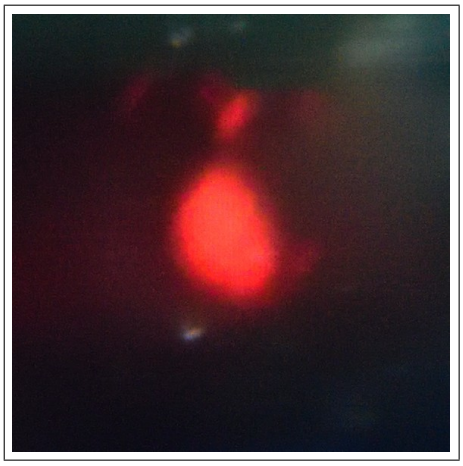

(b) 9th frame

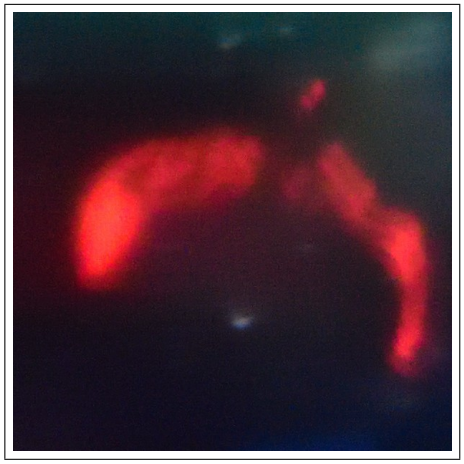

(c) 18th frame

(d) 36th frame

Fig. 5.9 Rotation animation generated by polygon-based method.

6

MIP-based CGH calculation method

In chapter 2, I have introduced the MIP. MIP is the simplest direct volume rendering method. And MIP is 2D image, lack of 3D scene. So, I applied a modified ray tracing method to reconstruct the 3D MIP. And then I applied the point light based CGH calculation method to generate the holograms.

In this chapter, I will introduce MIP-based CGH calculation method for volume

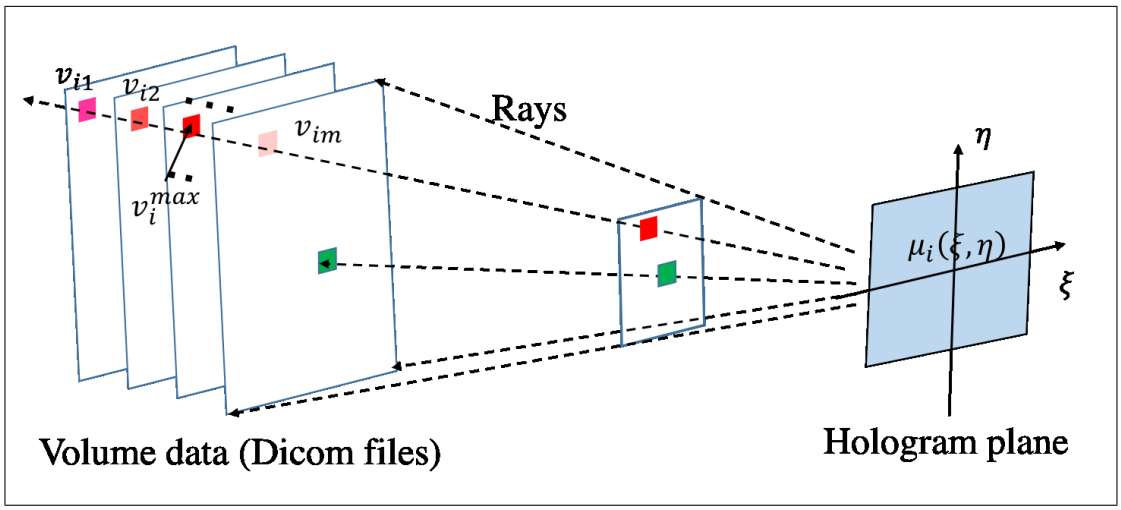

Fig. 6.1 CGH calculation with maximum intensity projection data.

data [14]. Section 6.1 will introduce the procedure of MIP-based method. Section 6.2 will introduce the MIP-based CGH calculation method in detail. Section 6.3 will introduce the experiments of MIP-based CGH calculation method.

6.1 Procedures of MIP-based method

The principle of MIP-based CGH calculation method was shown in Fig. 6.1. There are two operations in this method, the calculation of maximum intensity points and CGH calculation with MIP data.

For the first operation, I applied a modified ray tracing method to obtain the MIP data, which are the maximum voxel values of volume data. And the voxel values are normalize into 0 - 255.

For the second operation, I use the point light based CGH calculation method to generate the holograms with MIP data.

6.2 MIP-based CGH calculation method

In last chapter, I have introduced the polygon-based CGH calculation method. In polygon-based method, the ray tracing method was applied to obtain the point light sources, which are the intersections between polygonal models and rays. And ray tracing method render the polygonal model by Phong reflected equation. In this chapter, I try to apply the ray tracing method to generate holograms for MIP data. The previous ray tracing method is to obtain the closest intersections. And hidden surface removal can be realized. However, it is not suitable for MIP. In order to obtain the maximum voxel values, a modified ray tracing method was proposed as shown in Fig. 6.1. The ray tracing result of each ray will be the intersection with maximum value between the volume data and the ray as

$$v_i^{max} = max(v_{i1}, v_{i2}, ..., v_{im}), \tag{6.1}$$

where m is the number of volume slices (or the number of DICOM files), v_{ij} is the brightness of intersection between volume data j and ray i, and v_i^{max} is the brightness of maximum intersection of ray i.

By using modified ray tracing method, a series of points with maximum voxel values can be obtained. Each point is treated as a point light source. And the Eqs. 4.8 and 4.10 should be rewritten as

$$\mu_i(\xi, \eta) = \frac{v_i^{max}}{r_i} exp(-j(kr_i + \varphi_i)), \tag{6.2}$$

$$\mu(\xi,\eta) = \sum_{i=1}^{N} \mu_i(\xi,\eta), \tag{6.3}$$

where v_i^{max} is the amplitude of point light source i and φ_i is the random phase of point light source i. r_i is the compensated distance between the point light source i and the pixel (ξ,η) on the hologram plane as shown in Eq. 4.9.

6.3 Experiments

6.3.1 Experimental setup

In this chapter, experiments are performed on an electro-holographic display as shown in Fig. 5.4, the same with last chapter.

The parameters of the electro-holographic display and computer are shown in Tables 5.1 and 5.2, respectively. In this chapter, the experimental dataset includes two parts: the DICOM Image Library [52] and real patient data.

6.3.2 Reconstructed images

In this subsection, I perform two series of volume data to do experiments. The first series is lower limb angio (data type: MRI). The Fig.6.2(a) is the MIP image of this experiment. In this image, there are two parts: red and green parts. Figure 6.2(b) is the reconstructed image focusing on the green part. Figure 6.2(c) is the reconstructed image focusing on the red part. From Figs. 6.2(a) and 6.2(b), I can see that when the camera was focused on one data, the other appeared blurred. This indicated that the depths of red part and green part are different. And the reconstructed images display

Table 6.1 Computing times of polygon models shown in Fig.5.8 and Fig.6.3

	Skeleton	Visceral	Skeleton + Visceral	MIP
The number of vertices	345517	229872	585389	98825
The number of faces	686776	457702	1144478	
Computing time (s)	23.9	15.5	40.6	0.65

the depth correctly.

The second series is torso (data type: CT), which was also used in polygon-based CGH calculation method. I have talked about the polygon-based CGH calculation method in last chapter. Different with polygon-based method, MIP is the projection of maximum voxel values as described above , there is only one MIP of volume data from one direction as shown in Fig. 6.3(a). The reconstructed image of MIP-based CGH calculation method was shown in Fig. 6.3. The reconstructed image in Fig. 6.3(b) only supported single color.

6.3.3 Calculation time

In this subsection, there is an experiment about calculation time. This experiment is the computing time of the images shown in Fig. 5.8 and Fig. 6.3. And they are shown in Table. 6.1. The calculation speed of MIP-based CGH calculation method was at least 20 times faster than polygon-based method. And the calculation time of other other four sets of volume data was shown in Fig. 6.4. These volume data were skeleton, half-head, hands, and blood vessels. From Fig. 6.4, I determine that the MIP-based CGH calculation method was much faster than the polygon-based CGH calculation method.

6.3.4 Holographic animation

In this chapter, an electro-holographic display was applied. In Table 5.1, the refresh rate of SLM is 180 Hz. So, holographic animations are able to display on this device. Currently, MIP-based CGH calculation methods can generate holograms closed to real-time. A 36-frame rotation animation of a gallbladder was generated by MIP-based method.

Several frames generated by the MIP-based CGH calculation method are shown in Fig. 6.5. In the Fig. 6.5, sub-figures (a) and (c) are the reconstructed images from opposite directions. MIP-based CGH calculation method obtains the maximum values between rays and volume data, so the MIP results from opposite directions are symmetrical images as shown in Fig. 6.5.

The calculation time of MIP rotated animation is about 2.7 s, which was much faster than polygon-based method. If I use the latest GPU to accelerate the calculating speed, it is possible to realize the real-time animation.

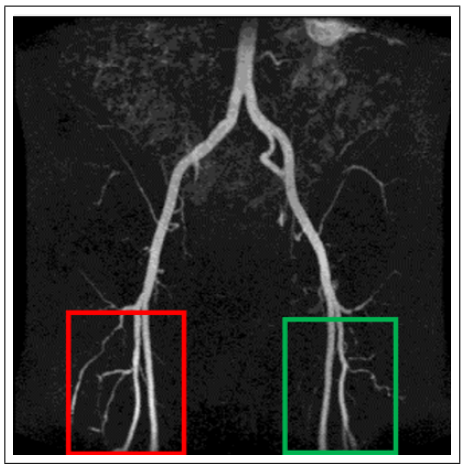

(a) MIP image of lower limb angio

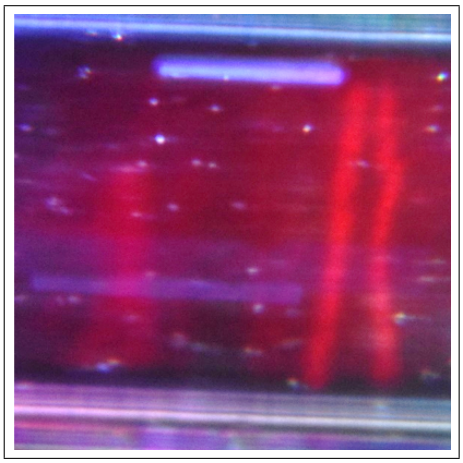

(b) Reconstructed image focusing on the green part

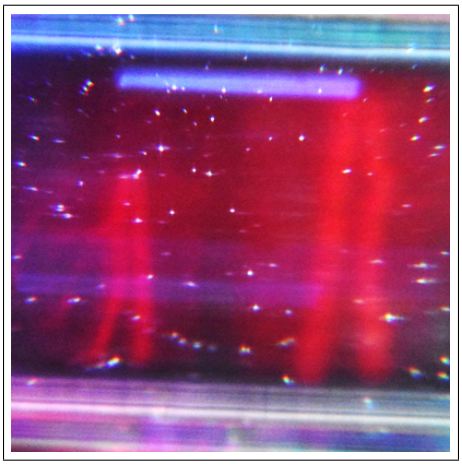

(c) Reconstructed image focusing on the red part

Fig. 6.2 MIP and reconstructed images.

(a) MIP

(b) Reconstructed image of MIP

Fig. 6.3 MIP and reconstructed image of torso.

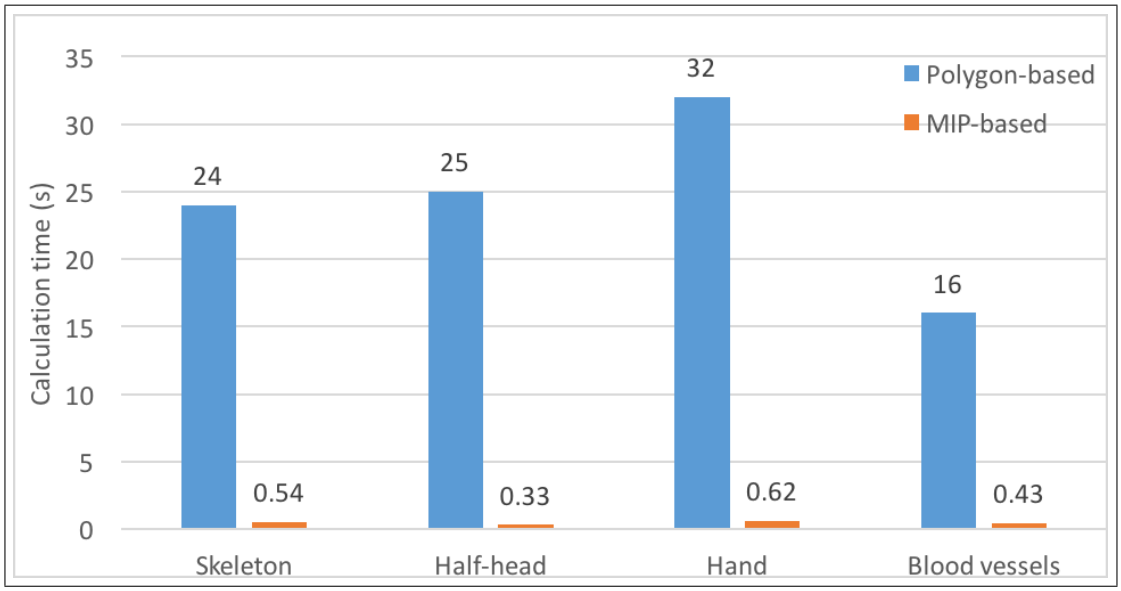

Fig. 6.4 Comparison of calculation times.

(a) 1st frame

(b) 9th frame

(c) 18th frame

(d) 36th frame

Fig. 6.5 Rotation animation generated by MIP-based method.

7

Volume rendering based CGH calculation method

In chapters 5 and 6, I have introduced two CGH calculation methods for volume data: polygon-based and MIP-based CGH calculation methods. Polygon-based CGH calculation method transformed the volume data to polygonal models firstly and then gen-

erated the holograms by ray tracing method. MIP-based CGH calculation method was the simplest volume rendering method to generate hologram data for volume data. However, the MIP-based method was just able to generate hologram data with high voxel values.

In this chapter, I will introduce volume rendering based CGH calculation method for volume data [15]. Section 7.1 will introduce the volume rendering based CGH calculation method. Section 7.2 will introduce an approximate CGH calculation method with elemental holograms for volume data. Section 7.3 will introduce the experiments of volume rendering based CGH calculation method.

7.1 Volume rendering based CGH calculation method

In last chapter, I have introduced the MIP-based CGH calculation method. The MIP-based method is the simplest directly volume rendering method to generate hologram data for volume data. However, MIP-based CGH calculation method has many limits, like lower image quality, unable to remove the hidden surface. In this section, I will introduce the volume rendering based CGH calculation method.

In volume rendering based CGH calculation method, there are three steps. First, initialize the color and opacity information based on the color map, α map, and voxel values. Color map and α map are designed by users depending on the object and imaging needs. There's no fixed maps for volume data. In this section, I applied the linear maps as example as shown in Fig. 7.1. Here, I represents the voxel value. C represents R, G, B, or α. For an unknown voxel x, the color or α value C_x is calculated by Eq. 7.1.

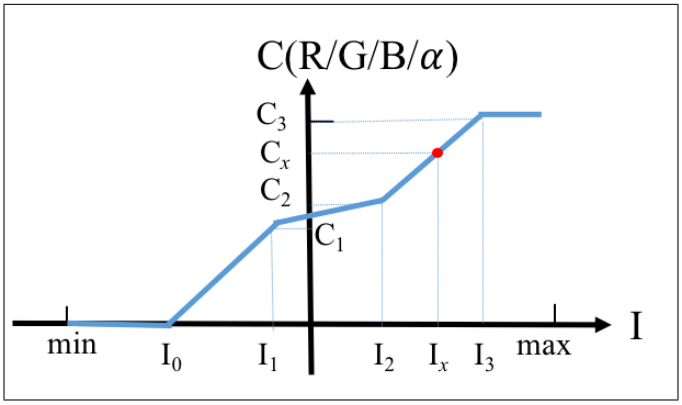

Fig. 7.1 Schematic diagram of color map and α map.

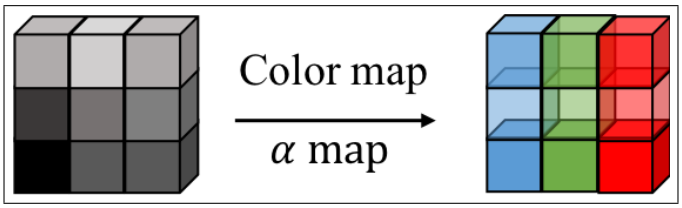

Fig. 7.2 Redefinition of R, G, B, and α based on color map and α map.

$$C_x = C_3 - \frac{(C_3 - C_2)(I_3 - I_x)}{(I_3 - I_2)}, \tag{7.1}$$

where C_2, C_3, I_2, and I_3 are the known values of the color map and α map. I_x is the value of $voxel_x$.

Based on this step, all voxels can be redefined with color and α information, as shown in Fig. 7.2.

Second step is the rendering step. I assumed that the reflection mode of volume data is the diffuse reflection. And I render all voxels with Lambertian equation in this step. In the CG area, the volume rendering result is a 2D image. Therefore, the value of each pixel is superposed by the rendering results of voxels. The volume rendering based CGH calculation method for volume data is different from CG volume ren-

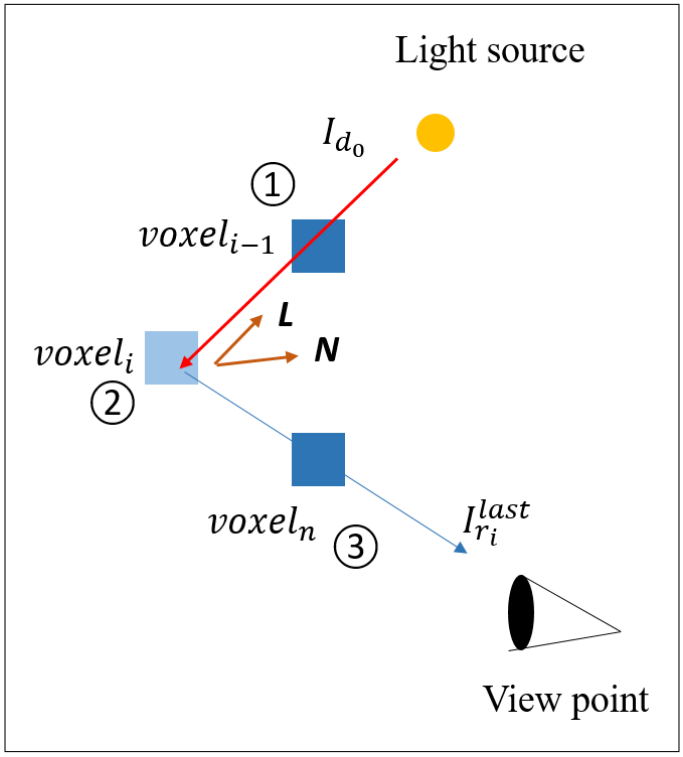

Fig. 7.3 Volume rendering method for single view point.

dering. CGHs record the wave information of 3D objects. So, the intensity value of reflected light and the position for each voxel should be considered.

For a single viewpoint, there are three processes in rendering step, as shown in Fig. 7.3. The first process is light propagation from the light source to $voxel_i$. The second process is the calculation of reflected light for $voxel_i$. The third process is light propagation from $voxel_i$ to the viewpoint. After fist step, each voxel has the$R$, G, B, and α information. And voxels can be treated as a series of transparent objects. Thus, the light propagation is accompanied by attenuation of light intensity.

I will apply $voxel_i$ as an example. In the first process, a ray propagates from the

light source to $voxel_i$. The attenuation equation is

$$I_{d_i} = I_{d_\circ} \prod_{j=0}^{i} (1 - \alpha_j), \tag{7.2}$$

where $I_{d_\circ}$ is the intensity of the light source, α_j is the opacity value of $voxel_j$, and I_{d_i} is the incident light of the second process. The principle of diffuse reflection is shown in Fig. 7.4. The intensity of the reflected light is calculated with the Lambertian model as follows:

$$I_{r_i} = k_{d_i} I_{d_i} max(0, \mathbf{L} \cdot \mathbf{N}), \tag{7.3}$$

where k_{d_i} corresponds to the ratio of Lambert light, and vector $\mathbf{L}$ is the unit vector to the light source. Vector $\mathbf{N}$ is the normal unit vector; its values are the gradient values of α in the x, y, and z directions. I_{r_i} is the intensity of reflected light. From Eq. 7.3 and Fig. 7.4, I can know that the intensity of reflected light does not depend on viewpoint position. After this process, the reflected ray propagates from $voxel_i$ to the viewpoint. And the attenuation equation is

$$I_{r_{Li}} = I_{r_i} \prod_{j=i+1}^{n} (1 - \alpha_j), \tag{7.4}$$

where $I_{r_{Li}}$ is the final reflected light intensity of $voxel_i$.

In theory, CGHs are multi-viewpoint images. For each voxel and each viewpoint, the intensity of diffuse reflected light are needed to be calculated as shown in Fig. 7.5. As I said above, the intensity of reflected light does not depend on viewpoint direction. Therefore, I_{d_i} and I_{r_i} are the same for all viewpoints. For each viewpoint, $I_{r_{Li}}$

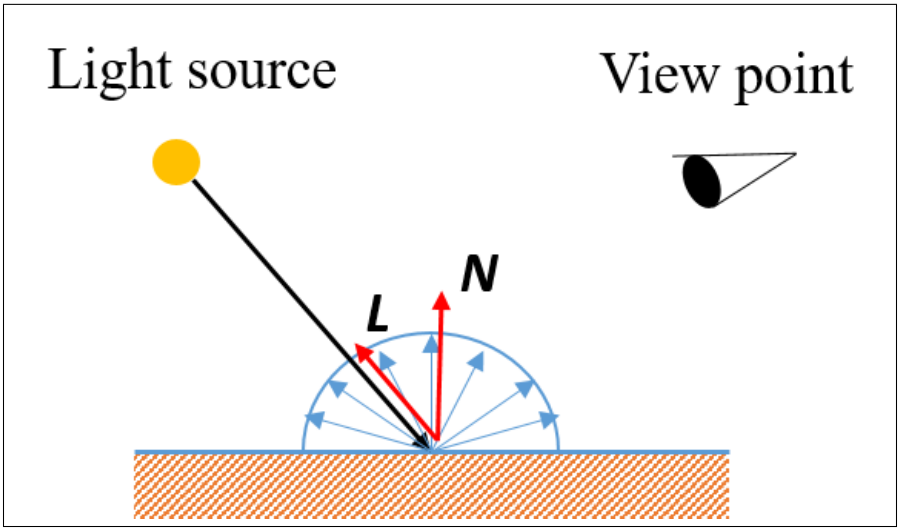

Fig. 7.4 Diffuse reflection model.

needs to be recalculated.

The last step is calculating the interference pattern for the rendered volume data. In this chapter, I applied the point light based method to generate hologram data. Every voxel can be treated as a point light source. For a point light source i, the complex amplitude distributions Eqs. 4.8 and 4.10 should be rewritten as

$$\mu_i(\xi, \eta) = \frac{I^n_{rLi}}{r_i} exp(-j(kr_i + \varphi_i)), \tag{7.5}$$

$$\mu(\xi, \eta) = \sum_{i=1}^{N} \mu_i(\xi, \eta), \tag{7.6}$$

where φ_i is the random phase of point light source i, and r_i is the distance between the point light source i and the pixel (ξ, η) on the hologram plane. I^n_{rLi} is the amplitude of point light source i for viewpoint n, which represents R, G, and B information. And

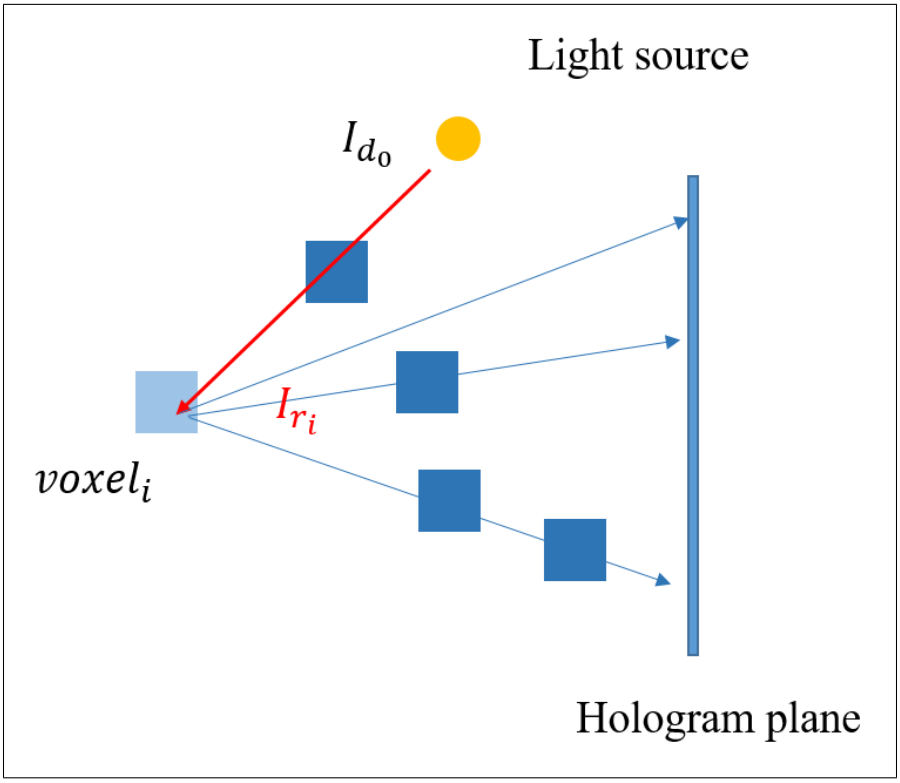

Fig. 7.5 CGH calculation with volume rendering method.

$I^n_{r_{Li}}$ is calculated with Eq. 7.4.

7.2 Approximate volume rendering based CGH calculation with elemental holograms

In last section, I have introduced the volume rendering based CGH calculation method for volume data. The calculation amount of volume rendering based CGH calculation is very large. If the number of voxels and hologram pixels are M and N, respectively, the computational complexity of incident light, reflected light and final light propagation will be $O(M^2)$, $O(M)$, and $O(M^2 \cdot N)$, respectively. And the computational complexity of the CGH calculation is $O(M \cdot N)$.

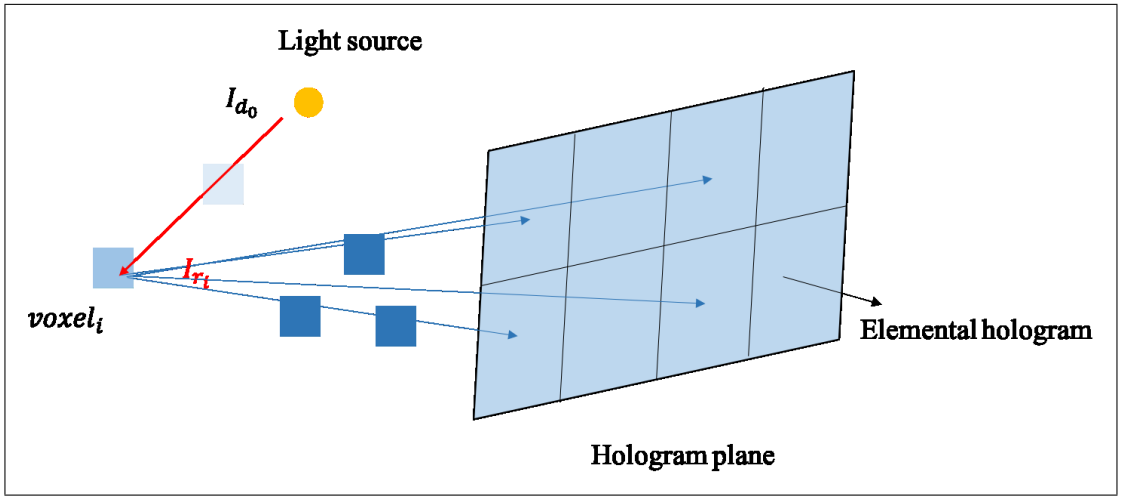

Fig. 7.6 CGH calculation with elemental holograms.

In order to increase the calculation time, an approximate volume rendering based CGH calculation method with elemental holograms was proposed. Dr. Ichikawa [36] also used the elemental holograms concept in his paper. He use the elemental holograms to show the stereo-holography. And the calculation speed of his CGH calculation method with elemental holograms is slower than his CGH calculation method without elemental holograms. When I calculate the reflected light intensity, I divide the hologram into several elemental holograms in this chapter, as shown in Fig. 7.6.

Unlike the last section, I have no need to calculate the final light propagation for $\mathcal{M}$ times. I can calculate it just once for each elemental hologram. Based on this idea, the computational complexity of the incident light, reflected light, and final light propagation for volume rendering based CGH calculation method with elemental holograms are $O(\mathcal{M}^2)$, $O(\mathcal{M})$, and $O(\mathcal{M}^2 \cdot N_e)$, respectively. The computational complexity of the CGH calculation is $O(\mathcal{M}^2 \cdot N)$. Here, $\mathcal{M}$ is the number of voxels, N is the number of hologram pixels, and N_e is the number of elemental holograms. In theory, the

CGH calculation time of two methods is the same. If N_e is small enough relative to N, the calculation time of final light propagation will be greatly shortened. And Eq. 6.2 should be rewritten as

$$\mu_i(\xi, \eta) = \frac{I_{r_{Li}}^{e_k}}{r_i} exp(-j(kr_i + \varphi_i)), \tag{7.7}$$

where $I_{r_{Li}}^{e_k}$ is the amplitude of point light source i for elemental hologram k. For each pixel in elemental hologram k, the amplitude of point light source i is the same.

7.3 Experiments

7.3.1 Experimental setup

In this chapter, experiments are performed on an electro-holographic display as shown in Fig. 5.4, the same with last chapter.

The parameters of the electro-holographic display and computer are shown in Tables 5.1 and 5.2, respectively. In this chapter, the experimental dataset includes three parts: the DICOM Image Library [52], real patient data, and DIY volume data.

7.3.2 Optical reconstructions

In this subsection, I gave an optical experiment. There are two data, and the geometry is shown in Fig. 7.7. The z coordinates of data1 and data2 are -50 cm and -100 cm, respectively. Fig. 7.8 shew the reconstructed images. From this figure, I determined that when the camera was focused on one data, the other appeared blurred. This indicated that these reconstructed images display the depth correctly.

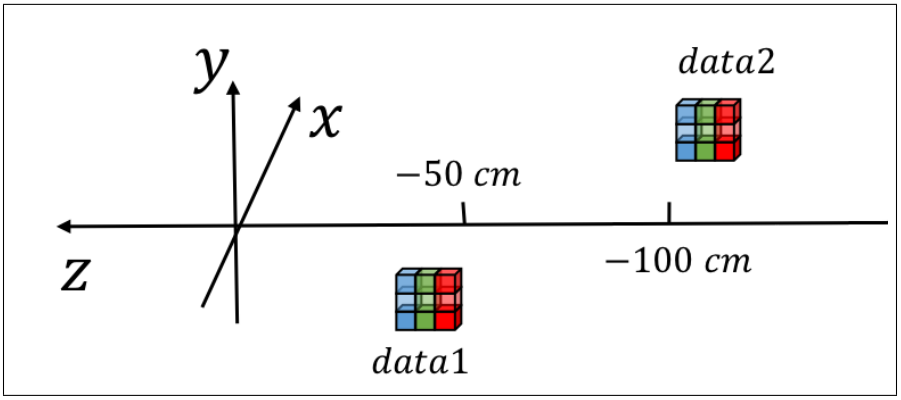

Fig. 7.7 Geometry for optical experiment.

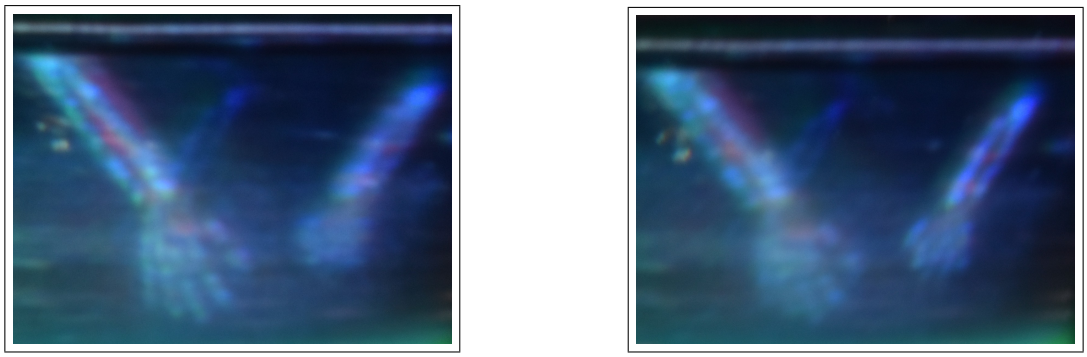

(a) Focusing on data1.

(b) Focusing on data2.

Fig. 7.8 Reconstructed images of optical experiment.

7.3.3 Approximate CGH calculation experiment

In this subsection, I performed an experiment to verify the validity of our approximate CGH calculation method, which was explained above. In this chapter, the volume rendering based CGH calculation method was called "VR method" for short, and the approximate volume rendering based CGH calculation method with elemental holograms was called "VR method with EH" for short. I applied 10×6 elemental holograms to perform the approximate calculation. In Fig. 7.9, 7.9(a) is the CG result,

Table 7.1 Calculation time

	Volume rendering	Volume rendering with EH
Rendering	24.3 h	3.6 h
CGH calculation	3.8 m	3.7 m
Total	24.3 h	3.6 h

7.9(b) is the reconstructed image of the VR method, and 7.9(c) is the reconstructed image of the VR method with EH. From Figs. 7.9(b) and 7.9(c), I determined that there were no major effects on the reconstructed images between the VR method and VR method with EH. And the calculation time can be greatly shortened, as shown in Table 7.1 .

7.3.4 Calculation time

In this subsection, there is an experiment about calculation time which between volume rendering based method and volume rendering based method with elemental holograms. As I said above, the calculation amount of the volume rendering based CGH calculation method is very large. And the volume rendering based CGH calculation method with EH was proposed to increase the calculation speed. In this subsection, I try to compare the calculation time of the two methods. Both of them have rendering and CGH calculation steps. I applied the gallbladder ($300 \times 300 \times 69$) to do this experiment. The number of elemental holograms is 10×6 in volume rendering based CGH method with EH. Table 7.1 shows the calculation time of two methods. In theory, the CGH calculation time of volume rendering based method and volume rendering based method with EH should be the same. Generally, the volume rendering based method with EH is 5 to 6 times faster than the volume rendering based method.

7.3.5 Reconstructed images

In this subsection, I perform three series of volume data to do experiments. The first series of volume data is called VIX (data type: CT). In this experiment, I try to generate the hologram data for transparent objects. Figures 7.10(a) and 7.10(c) are the CG rendering results. Figures 7.10(c) and 7.10(d) are the reconstructed images. Fig. 7.10(b) shows the reconstructed image of bone, which was an opacity object. Fig. 7.10(d) shows the reconstructed image of feet, and I can see the bone through transparent skin. From this experiment, I can determine that volume rendering based CGH calculation method can generate the hologram data for transparent objects.

I generated a series of volume data by myself to discuss the rendering results with different α maps. I try to apply different α maps to generate hologram data with volume rendering based CGH calculation method. And the reconstructed images are shown in Fig. 7.11. In this experiment, the green ball is an opacity object and the red cube is a transparent object. Fig. 7.11(a) - 7.11(d) are the reconstructed images with different α maps. The transparency changes of the red object are clearly displayed.

The third experimental series of volume data is called Cenovix (data type: CT). In this experiment, I applied volume rendering based method to generate the hologram data for multi-layer objects. In Fig. 7.12, there are three objects: bone, visceral tissue, and metal. Figure 7.12(b) is the reconstructed image of this experiment. Due to the low resolution of the device, the reconstructed image is not very clear. I can see multiple objects in Fig. 7.12(b). Based on this experiment, volume rendering based CGH calculation method can generate the multi-layer objects.

(a) CG result.

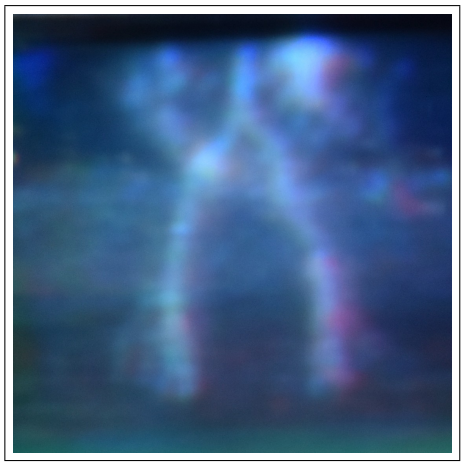

(b) Reconstructed image of VR method.

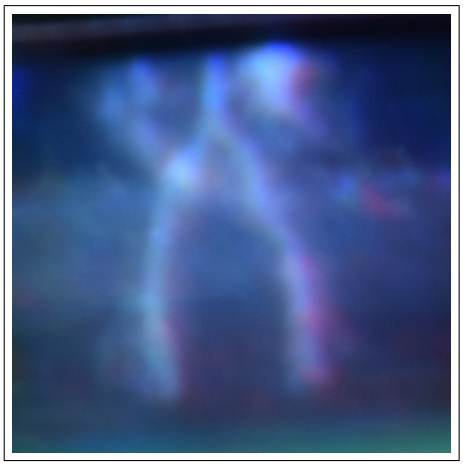

(c) Reconstructed image of VR method with EH.

Fig. 7.9 Reconstructed images of approximate experiment.

(a) CG result

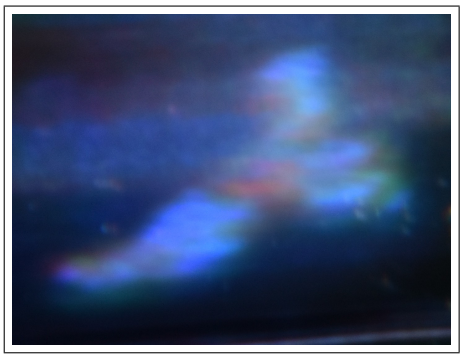

(b) Opacity object

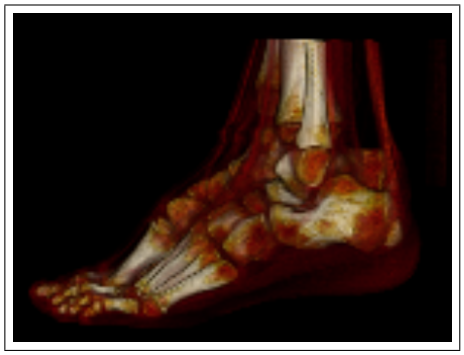

(c) CG result

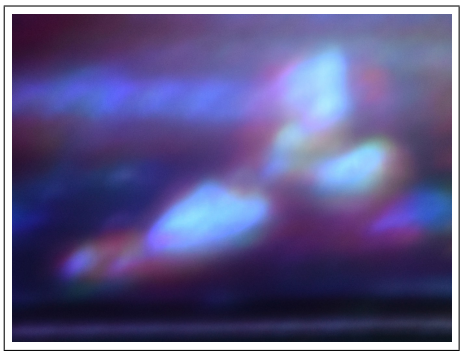

(d) Transparent object

Fig. 7.10 Reconstructed images of VIX (transparent objects).

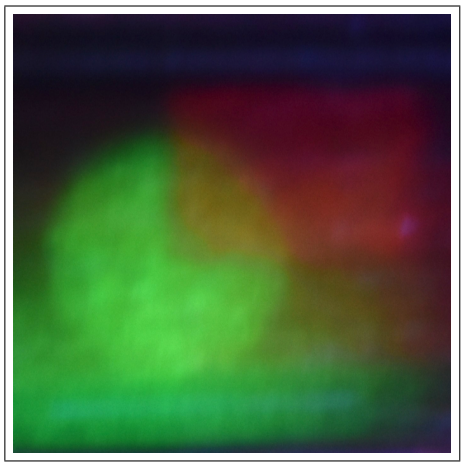

(a) α_G: 0.8, α_R: 0.08

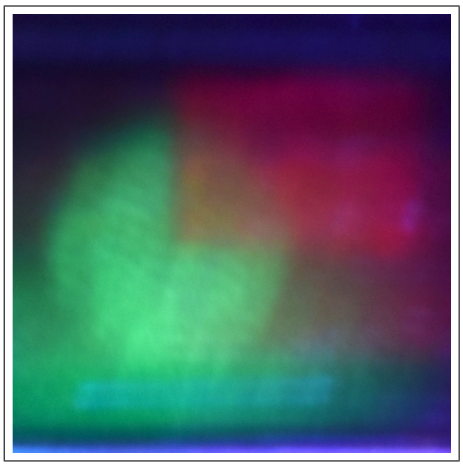

(b) α_G: 0.8, α_R: 0.12

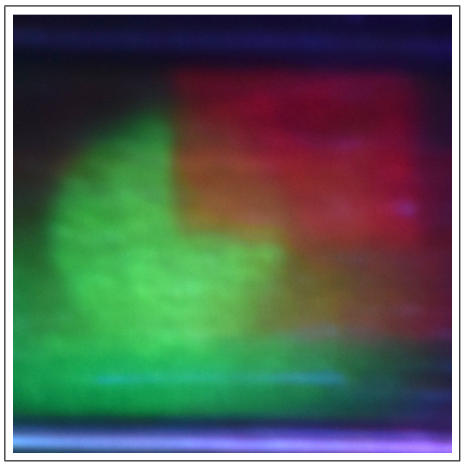

(c) α_G: 0.8, α_R: 0.2

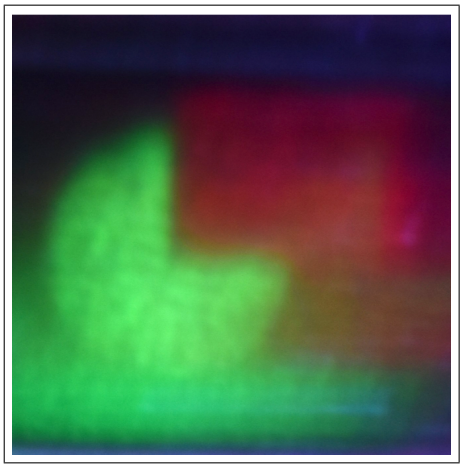

(d) α_G: 0.8, α_R: 0.5

Fig. 7.11 Reconstructed images of transparent object with different α maps. (a), (b), (c), and (d) are reconstructed images with different α maps.

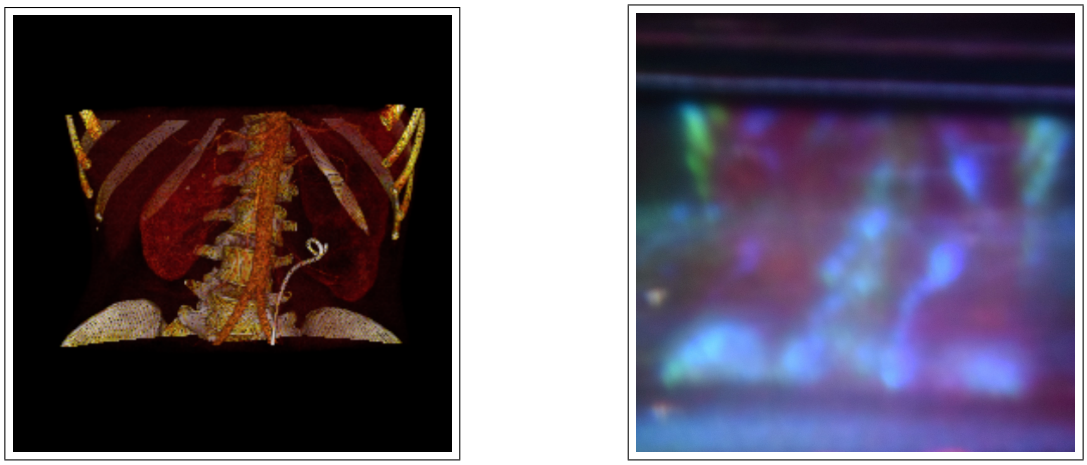

(a) Multi-layer object

(b) Reconstructed image

Fig. 7.12 Reconstructed images of multi-layer objects. (a) is CG rendering result of multi-layer objects. (b) is reconstructed image of multi-layer objects.

8

Discussion

In this thesis, I have introduced three CGH calculation method for volume data in previous chapters. And several experiments have been carried out. In this chapter, I will discuss the usage and differences of each method. And I will discuss the reconstructed images and calculation time of three methods in section 8.1 and section 8.2, respectively. In section 8.3, I will summarize the three CGH calculation methods for volume

data.

8.1 Discussion of reconstructed images

In chapters 5, 6, and 7, I gave several experiments. Many reconstructed images have shown in these figures. I discussed some differences in last section. In this section, I will discuss the reconstructed images of three CGH calculation methods.

In this section, I use the series of volume data for this experiment which is called gallbladder (data type: MRI). In this experiment, I applied polygon-based, MIP-based, and volume rendering based methods as comparative tests. The voxel values of the gallbladder are relatively large. Therefore, i can obtain similar results by these three methods, as shown in Fig. 8.1. From this figure, I determined that these three methods can be used to generate hologram data for volume data. And the detail of Fig. 8.1(d) is better than that of the other two methods.

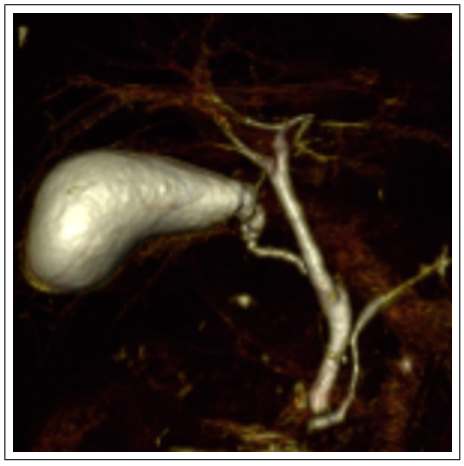

(a) CG result

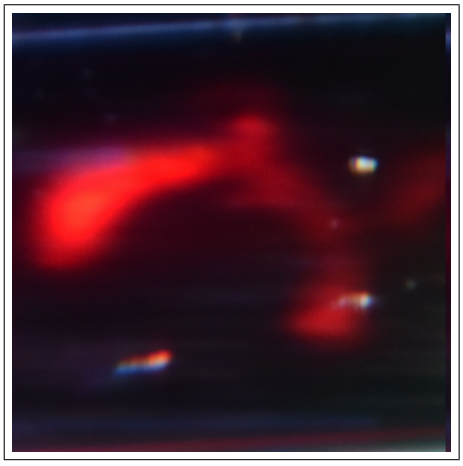

(b) Polygon-based method

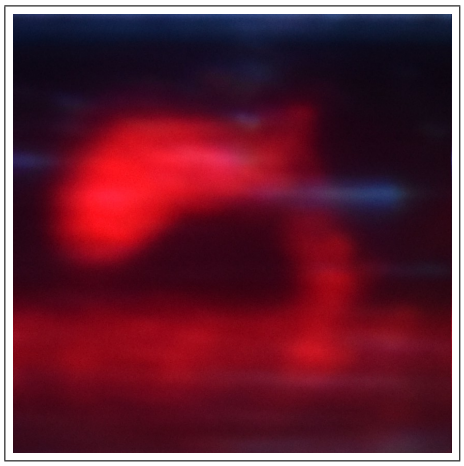

(c) MIP-based method

(d) Volume rendering based method with EH

Fig. 8.1 Reconstructed images of different method. (a) is the CG rendering result. (b) is the reconstructed image of polygon-based method. (c) is the reconstructed image of MIP-based method. (d) is the reconstructed image of volume rendering based method with EH.

8.2 Discussion of calculation time

In sections 6.3 and 7.3, there are two experiments about calculation time. From the Fig. 6.4 and Table 6.1, we can know that MIP-based CGH calculation method is much faster than polygon-based CGH calculation method. And the time spent by polygon-based and MIP-based methods can be calculated in seconds. This indicates that the calculation time of MIP-based method can be closed to real-time and the calculation of polygon-based method is fast enough.

The Table 7.1 has shown the calculation time of volume rendering based CGH calculation methods. From this table, we can know that the calculation time of volume rendering based CGH calculation method is calculated by hours. And the volume rendering based CGH calculation with elemental holograms is 5 to 6 times faster than volume rendering based CGH calculation method.

In this section, there is an new experiment about calculation time which among all four methods. Data are the same with Table 7.1. And the number of voxels is 300 $\times$ 300 $\times$ 69. In this experiment, I discuss the calculation time of the four methods. The polygon-based method, MIP-based method, and volume rendering based method all contain two steps: rendering and CGH calculation. Of course, the polygon-based method should generate the polygon data before these two steps. Table 8.1 shows the calculation time of the different methods. The number of elemental holograms is 10 $\times$ 6 elements in the volume rendering based method with EH. All the calculation time results of Table 8.1 are the averages of ten calculations. From this table, I determined that the volume rendering based CGH calculation method and volume rendering based

Table 8.1 Calculation time of different methods

	Polygon-based	MIP-based	VR-based	VR-based with EH
Rendering	1.5 s	0.2 s	24.3 h	3.6 h
CGH calculation	0.3 s	0.6 s	3.8 m	3.7 m
Total	1.8 s	0.8 s	24.3 h	3.6 h

CGH calculation method with EH take more time to do the rendering step than the polygon-based and MIP-based methods. And the polygon-based method and MIP-based method are far faster than the other two methods. The MIP-based method can achieve real-time computing with the latest GPU.

8.3 Summary of three methods

In this thesis, I have introduced three CGH calculation methods for volume data: polygon-based method, MIP-based method, and volume rendering based method. The polygon-based method should generate the polygonal models before rendering and CGH calculation. MIP-based method and volume rendering based method are the directly rendering method.

All three methods can generate clear holograms for volume data. And each of the three methods has advantages and disadvantages. Polygon-based CGH calculation method can combine the models by using 3D editing software. And I can generate the holograms with material information by using polygon-based CGH calculation method. Manual operations of polygon-based method can increase the diversity of holograms for volume data while also increasing the difficulty of hologram generation. MIP-based CGH calculation used the simplest direct volume rendering method and point light-based method to generate holograms for volume data. The calculation

speed of MIP-based method is closed to real-time. However, the general holograms generated by MIP-based method are single color images. Different with polygon-based and MIP-based CGH calculation methods, volume rendering based CGH calculation method can generate the best quality of holograms. And volume rendering based CGH calculation method can generate the transparent objects and multi-layer objects. However, the calculation speed is very slow. To increase the calculation speed, an approximate volume rendering based CGH calculation method with elemental holograms was proposed.

From a series of volume data, MIP-based CGH calculation method can only generate one hologram. Different with MIP-based method, polygon-based method and volume rendering based method can generate several holograms. MIP-based method aims to show the object with high voxel values. So, MIP-based method can be applied in the field of medical diagnosis and meteorological analysis. Of course, polygon-based method and volume rendering based method can be applied too. However, they are more suitable for medical simulation and model display, such as surgical simulation, medical education, and digital sand table. Holography was proposed as an ideal 3D display technology. And voxgram system has proved that holographic display method is better than CG display for medical data. Although the current holography is still in the scientific research stage, it has not been applied to the corresponding fields. I believe that there will be many holographic applications in the near future. And my CGH calculation methods for volume data will be used.

9

Conclusion

In this thesis, I proposed three CGH calculation methods for volume data : polygon-based, MIP-based, and volume rendering based methods. In the polygon-based method, there are two operations: surface extraction and CGH calculation. I first extract the ios-surfaces from the volume data. And then I applied the ray tracing CGH calculation method to generate the holograms. The MIP-based CGH calculation method used

a modified ray tracing method and point light based CGH calculation method to generates holograms with maximum voxel values. In volume rendering based method, I attempted to apply the diffuse reflection model to render the volume data. I calculated the CGHs for volume data using a point light based CGH method. To increase the calculation speed of volume rendering based CGH calculation method, an approximate volume rendering based CGH calculation method with elemental holograms was proposed.

In this thesis, an electro-holographic display was used as reconstruction device. And holographic animations are possible to be displayed. All three methods can display the depth well. The polygon-based method can generate clear holograms for volume data. And the polygonal models can be combined and edited by using 3DCG software. By using polygon-based CGH calculation method, the color and material of polygonal models can be designed independently. Different with polygon-based CGH calculation method, MIP-based CGH calculation method can only generate single color holograms. And MIP-based CGH calculation is just suit to the objects with high voxel values. The volume rendering based CGH calculation method can generate the holograms for the transparent objects and multi-layer objects well. Compared with polygon-based and MIP-based CGH calculation methods, the quality of holograms calculated by the proposed method is better.

For the computing speed, the MIP-based CGH calculation method is much faster than other two methods. It was possible to generate the CGHs in real-time by using the latest GPUs. The calculation time of volume rendering based method is very long. To increase the calculation speed of volume rendering based method, an approximate

volume rendering based CGH calculation method with elemental holograms was proposed.

By using my CGH calculation methods, various volume data can be displayed in an effective way, including those in the medical field.

Acknowledgments

I would like to express my sincere gratitude to my advisor Prof. Yuji Sakamoto for the continuous support of my Ph.D study and related research, for his patience, motivation, and immense knowledge. His guidance helped me in all the time of research and writing of this thesis.

Besides my advisor, I would like to thank the rest of my deputy advisors: Prof. Tsuyoshi Yamamoto, Prof Kenji Araki, and Prof. Miki Haseyama, for their insightful comments and encouragement, but also for the hard question which incented me to widen my research from various perspectives.

My sincere thanks also goes to assistant professor Seok Kang, who has given me a lot of help. He gave me a lot of convenience during the doctoral course.

I thank my fellow labmates for their help in study and life. As an international student in Japan, it's really lucky to be able to get help from others. During the doctoral course, we did the research together and learned from each other.

Last but not the least, I would like to thank my family: my parents, my wife and my daughter for supporting me spiritually throughout writing this thesis and my life in general.

Research achievements

Journals

- Zixiang Lu and Yuji Sakamoto, “Holographic display methods for volume data: polygon- based and MIP-based methods,” Applied Optics, Vol. 57, Issue 1, pp. A142-A149 (2018).
- Zixiang Lu and Yuji Sakamoto, “Holographic display method for volume data by volume rendering,” Optics Express, Vol. 27, Issue 2, pp. 543-556 (2019).

International conferences

- Zixiang Lu and Yuji Sakamoto, “A Holographic Display Method of Medical Images with Modified Ray Tracing Method,” Digital Holography and Three-Dimensional Imaging, OSA Technical Digest (Optical Society of America), paper M3B.4, May. 2017.
- Zixiang Lu and Yuji Sakamoto, “A Holographic Display method of Maxi-

mum Intensity Projection of Medical Image by Electro-holography," The Sixth Japan-Korea Workshop on Digital Holography and Information Photonics, p20-30, Dec.2016

Others

- Zixiang Lu and Tadahiro Fujimoto, "Iterative refinement of alpha matte using binary classifier," The Journal of Society for Art and Science, Vol. 14, No. 5, pp.207-219 (2015).

References

[1] J. A. Maintz and M. A. Viergever, "A survey of medical image registration," *Medical Images Analysis*, vol. 2, no. 1, pp. 1–36, 1998.

[2] M. Levoy, "Display of surfaces from volume data," *IEEE Computer Graphics and Applications*, vol. 8, pp. 29–37, 1998.

[3] S. Napel, M. P. Marks, G. D. Rubin, M. D. Dake, C. H. McDonnell, S. M. Song, D. R. Enzmann, and J. R B Jeffrey, "CT angiography with spiral CT and maximum intensity projection," *Radiology*, vol. 185, no. 2, pp. 607–610, 1992.

[4] Drebin, R. A., L. Carpenter, and P. Hanrahan, "Volume rendering," *ACM Siggraph Computer Graphics*, vol. 22, no. 4, pp. 65–74, 1998.

[5] J. Kruger and R. Westermann, "Acceleration techniques for gpu-based volume rendering," in *Proceedings of the 14th IEEE Visualization 2003 (VIS'03)*, VIS '03, pp. 38–43, Washington, DC, USA: IEEE Computer Society, 2003.

[6] E. N. Leith and J. Upatnieks, "Reconstructed wavefronts and communication theory," *J. Opt. Soc. Am*, vol. 53, pp. 1123–1130, 1962.

[7] D. Gabor, "A new microscopic principle," *Nature*, vol. 161, pp. 777–778, 1948.

[8] L. H. Lin and H. L. Beauchamp, "Write-read-erase in situ optical memory using thermoplastic holograms," *Applied Optics*, vol. 9, pp. 2088–2092, 1970.

[9] X. Zhang, E. Dalsgaard, S. Liu, H. Lai, and J. Chen, "Concealed holographic coding for security applications by using a moiré technique," *Appl. Opt.*, vol. 36, pp. 8096–8097, Nov 1997.

[10] A. Wolfe and S. Hart, "Digital volumetric holograms for medical imaging." `http://spie.org/newsroom/digital-volumetric-holograms-for-medical-imaging`.

[11] C. Honda, S. Takahashi, S. J. Hart, and R. J. Rankin, "The technology in the digital holography system," *Japan Science and Technology Information Aggregator, Electronic*, vol. 15, no. 3, pp. 135–145, 1998.

[12] J. Khan, "Static digital holograms for medical images." http://www.holoxica.com/digital-holograms/.

[13] Y. Sakamoto, T. Aoyama, and Y. Aoki, "Volume rendering for computer generated holograms," in *Proceedings of 19th International Commission for Optics (ICO-19)*, pp. 555–556, 2002.

[14] Z. Lu and Y. Sakamoto, "Holographic display methods for volume data: polygon-based and mip-based methods," *Appl Opt*, vol. 57, no. 1, pp. A142–A149, 2018.

[15] Z. Lu and Y. Sakamoto, "Holographic display method for volume data by volume rendering," *Opt. Express*, vol. 27, pp. 543–556, Jan 2019.

[16] DICOM PS3.1 2018d - Introduction and Overview. http://dicom.nema.org/medical/dicom/current/output/chtml/part01/chapter_1.html.

[17] OsiriX, "The world famous dicom viewer." http://www.osirix-viewer.com/.

[18] ImageJ, "Image processing and anglysis in java." https://imagej.net/Welcome.

[19] The Visualization Toolkit. http://www.vtk.org/.

[20] Insight Segmentation and Registration Toolkit. http://www.itk.org/.

[21] MathWorks - MATLAB/Simulink. https://jp.mathworks.com/.

[22] Lorensen, W. E., and H. E. Cline, "Marching cubes: A high resolution 3d surface construction algorithm," *ACM SIGGRAPH Computer Graphics*, vol. 21, no. 4, pp. 163–169, 1987.

[23] Audtodesk 3ds Max. http://www.autodesk.com.

[24] Meshlab. http://www.meshlab.net/.

[25] Blender – Free and Open 3D creation software. https://www.blender.org/.

[26] NVIDIA ACCELERATED COMPUTING. https://www.nvidia.com/ja-jp/.

[27] Y. Sando, D. Barada, B. J. Jackin, and T. Yatagai, "Fast calculation method for computer-generated cylindrical holograms based on the three-dimensional fourier spectrum," *Opt. Lett.*, vol. 38, pp. 5172–5175, Dec 2013.

[28] R. H.-Y. Chen and T. D. Wilkinson, "Computer generated hologram with geometric occlusion using gpu-accelerated depth buffer rasterization for three-dimensional display," *Appl. Opt.*, vol. 48, pp. 4246–4255, Jul 2009.

[29] A. P. Goutzoulis, "Fast fourier transforms with factored residue look-up tables," *Appl. Opt.*, vol. 28, pp. 4167–4175, Oct 1989.

[30] S.-C. Kim, J.-K. Lee, and E.-S. Kim, "Fast generation of computer generated hologram with reduced look-up table," in *Adaptive Optics: Analysis and Methods/Computational Optical Sensing and Imaging/Information Photonics/Signal Recovery and Synthesis Topical Meetings on CD-ROM*, p. DTuB7, Optical Society of America, 2007.

[31] S.-C. Kim and E.-S. Kim, "Effective generation of digital holograms of three-dimensional objects using a novel look-up table method," *Appl. Opt.*, vol. 47, pp. D55–D62, Jul 2008.

[32] C. Gao, J. Liu, X. Li, G. Xue, J. Jia, and Y. Wang, "Accurate compressed look up table method for cgh in 3d holographic display," *Opt. Express*, vol. 23, pp. 33194–33204, Dec 2015.

[33] Y. Ogihara and Y. Sakamoto, "Fast calculation method of a cgh for a patch model using a point-based method," *Appl. Opt.*, vol. 54, pp. A76–A83, Jan 2015.

[34] T. Sugawara, Y. Ogihara, and Y. Sakamoto, "Fast point-based method of a computer-generated hologram for a triangle-patch model by using a graphics processing unit," *Appl. Opt.*, vol. 55, pp. A160–A166, Jan 2016.

[35] K. Wakunami and M. Yamaguchi, "Calculation for computer generated hologram using ray-sampling plane," *Opt. Express*, vol. 19, pp. 9086–9101, May 2011.

[36] T. Ichikawa, K. Yamaguchi, and Y. Sakamoto, “Realistic expression for full-parallax computer-generated holograms with the ray-tracing method,” *Applied Optics*, vol. 52, pp. 201–209, 2013.

[37] K. Matsushima, “Computer-generated holograms for three-dimensional surface objects with shade and texture,” *Appl. Opt.*, vol. 44, pp. 4607–4614, Aug 2005.

[38] R. Watanabe, K. Yamaguchi, and Y. Sakamoto, “Fast calculation method of computer generated hologram animation for viewpoint parallel shift and rotation using fourier transform optical system,” *Appl. Opt.*, vol. 55, pp. A167–A177, Jan 2016.

[39] S. H. Lee, S. C. Kwon, H. B. Chae, J. Y. Park, H. J. Kang, and J. D. K. Kim, “Digital hologram generation for a real 3d object using by a depth camera,” *Journal of Physics: Conference Series*, vol. 415, no. 1, p. 012049, 2013.

[40] E.-Y. Chang, J. Choi, S. Lee, S. Kwon, J. Yoo, M. Park, and J. Kim, “360-degree color hologram generation for real 3d objects,” *Appl. Opt.*, vol. 57, pp. A91–A100, Jan 2018.

[41] T. Yoneyama, C. Yang, Y. Sakamoto, and F. Okuyama, “Eyepiece-type full-color electro-holographic binocular display with see-through vision,” in *Proceedings of Digital Holography and Three-Dimensional Imaging*, p. DW2A.11, Optical Society of America, 2013.

[42] Y. Takaki and S. Uchida, “Table screen 360-degree three-dimensional display using a small array of high-speed projectors,” *Opt. Express*, vol. 20, pp. 8848–8861, Apr 2012.

[43] X. Xia, X. Liu, H. Li, Z. Zheng, H. Wang, Y. Peng, and W. Shen, “A 360-degree floating 3d display based on light field regeneration,” *Opt. Express*, vol. 21, pp. 11237–11247, May 2013.

[44] T. Inoue and Y. Takaki, “Table screen 360-degree holographic display using circular viewing-zone scanning,” *Opt. Express*, vol. 23, pp. 6533–6542, Mar 2015.

[45] Y. Lim, K. Hong, H. Kim, H.-E. Kim, E.-Y. Chang, S. Lee, T. Kim, J. Nam, H.-G. Choo, J. Kim, and J. Hahn, “360-degree tabletop electronic holographic display,” *Opt. Express*, vol. 24, pp. 24999–25009, Oct 2016.

[46] E. MURAKAMI, Y. OGURO, and Y. SAKAMOTO, "Study on compact head-mounted display system using electro-holography for augmented reality," *IEICE Transactions on Electronics*, vol. E100.C, no. 11, pp. 965–971, 2017.

[47] A. Maimone, A. Georgiou, and J. S. Kollin, "Holographic near-eye displays for virtual and augmented reality," *ACM Trans. Graph.*, vol. 36, pp. 85:1–85:16, July 2017.

[48] Y. O. H. K. K. Y. Y. S. Takuo Yoneyama, Eishin Murakami, "Holographic head-mounted display with correct accommodation and vergence stimuli," *Optical Engineering*, vol. 57, pp. 57 – 57 – 9, 2018.

[49] G. W. Stroke, "Lensless fourier-transform method for optical holography," *Appl. Phys. Lett.*, vol. 6, pp. 201–203, 1965.

[50] T. Ichikawa, T. Yoneyama, and Y. Sakamoto, "Cgh calculation with the ray tracing method for the fourier transform optical system," *Opt. Express*, vol. 21, pp. 32019–32031, Dec 2013.

[51] T. Shimobaba and T. Ito, "A color holographic reconstruction system by time division multiplexing with reference lights of laser," *Optical Review*, vol. 10, pp. 339–341, 2003.

[52] DICOM Image Library. http://www.osirix-viewer.com/resources/dicom-image-library/.